Article:

Meek, U, Piazolo, S orcid.org/0000-0001-7723-8170 and Daczko, NR (2019) The field and microstructural signatures of deformation-assisted melt transfer: Insights from magmatic arc lower crust, New Zealand. Journal of Metamorphic Geology, 37 (6). pp. 795-821. ISSN 0263-4929

https://doi.org/10.1111/jmg.12488

The field and microstructural signatures of deformation-assisted melt transfer: Insights from magmatic arc lower crust of New Zealand

Journal:	*Journal of Metamorphic Geology*
Manuscript ID	JMG-18-0049.R2
Manuscript Type:	Original Article
Date Submitted by the Author:	n/a
Complete List of Authors:	Meek, Uvana; Macquarie University, Department of Earth and Planetary Sciences Piazolo, Sandra; Macquarie University, Department of Earth and Planetary Sciences; University of Leeds, School of Earth and Environment Daczko, Nathan; Macquarie University, Department of Earth and Planetary Sciences
Keywords:	reactive melt flow, dissolution-precipitation, melt-rock interaction, hornblendite

THE FIELD AND MICROSTRUCTURAL SIGNATURES OF DEFORMATION-ASSISTED MELT TRANSFER: INSIGHTS FROM MAGMATIC ARC LOWER CRUST, NEW ZEALAND

U. Meek, S. Piazolo, N. R. Daczko

Australian Research Council Centre of Excellence for Core to Crust Fluid Systems (CCFS) and GEMOC, Department of Earth and Planetary Sciences, Macquarie University, Sydney, NSW 2109, Australia

Short title: Channelized reactive melt flow in lower crust

ABSTRACT

Melt must transfer through the lower crust, yet the field signatures and mechanisms involved in such transfer zones (excluding dykes) are still poorly understood. We report field and microstructural evidence of a deformation-assisted melt transfer zone that developed in the lower crustal magmatic arc environment of Fiordland, New Zealand. A 30–40m wide hornblende-rich body comprising hornblende ± clinozoisite and/or garnet exhibits 'igneous-like' features and is hosted within a metamorphic, two-pyroxene-pargasite gabbroic gneiss. Previous studies have interpreted the hornblende-rich body as an igneous cumulate or a mass transfer zone. We present field and microstructural characteristics supporting the later and indicating the body has formed by deformation-assisted, channelized, reactive porous melt flow. The host granulite facies gabbroic gneiss contains distinctive rectilinear dykes and garnet reaction zones (GRZ) from earlier in the geological history; these form important reaction and strain markers. Field observations show that the mineral assemblages and microstructures of the gabbroic gneiss and GRZ are progressively modified with proximity to the hornblende-rich body. At the same time GRZ bend systematically into the hornblende-rich body on each side of the unit, showing apparent sinistral shearing. Within the hornblende-rich body itself, microstructures and EBSD mapping show evidence of the former presence of melt including observations consistent with melt crystallisation within pore spaces, elongate pseudomorphs of melt films along grain boundaries, minerals with low dihedral angles <10–<60º, and interconnected 3D melt pseudomorph networks. Reaction microstructures with highly irregular contact boundaries are observed at the field and thin-section scale in remnant islands of original rock and replaced grains, respectively. We infer that the hornblende-rich body was formed by modification of the host gabbroic gneiss in-situ due to reaction between an externally-derived, reactive, hydrous gabbroic to intermediate melt percolating via porous melt flow through an actively deforming zone. Extensive melt-rock interaction and metasomatism occurred via coupled dissolution-precipitation, triggered by chemical disequilibrium between the host rock and the fluxing melt. As a result, the host plagioclase and pyroxene became unstable and were reacted and dissolved into the melt, while hornblende and to a lesser extent clinozoisite and garnet grew replacing the unstable phases. Our study shows that hornblendite rocks commonly observed within deep crustal sections, and attributed to cumulate fractionation processes, may instead delineate areas of deformation-assisted, channelized reactive porous melt flow formed by melt-mediated coupled dissolution-precipitation replacement reactions.

Keywords: reactive melt flow, dissolution-precipitation, melt-rock interaction, hornblendite

INTRODUCTION

It is well established that heat transfer from the Earth's mantle to the surface is crucial for continental differentiation and driving plate tectonics, and thus must involve significant mass transfer (via migration of melt) through the crust (Bercovici, 2003; Brown, 2010; Gurnis, 1988; Schubert, Turcotte, & Olson, 2001). Our understanding of the mechanisms of melt transfer in crustal zones is limited to channelled melt transfer through dykes and melt-bearing shear zones, yet the number and volume of these pathways are too small to accommodate the heat and mass transfer necessary for chemical differentiation (Rudnick, 1995). Pervasive melt movement (Brown, 2010; Hasalová, Schulmann, et al., 2008a; Sawyer, 1999; Weinberg, 1999) is not well understood, but may explain the discrepancy between recognized former melt pathways and necessary melt transfer needed within our Earth system. This discrepancy focusses attention on an existing gap in our ability to identify former melt pathways in the geological record.

To identify these cryptic melt pathways, indicative field relationships and microstructures need to be established. While the signatures related to melt flux through dykes (Sleep, 1988; Spence, Sharp, & Turcotte, 1987; Weinberg, 1996) or melt-bearing shear zones (Beach & Fyfe, 1972; Carter & Dworkin, 1990; Cartwright & Barnicoat, 2003; Lee, Torvela, Lloyd, & Walker, 2018; Streit & Cox, 1998; Stuart, Piazolo, & Daczko, 2018) have been well-documented in the continental crust, those associated with the third possible pervasive movement mechanism of porous melt flow, are largely lacking. The latter process involves melt flow along grain boundaries and within grain triple junctions, where the melt forms a highly connected network (Scott & Stevenson, 1986; Turcotte & Ahern, 1978). This contrasts to easily recognised field relationships where melt segregated to form a dyke or in the case of shear zones that preserve a high proportion of crystallised melt (Vanderhaeghe, 1999; Weinberg & Searle, 1998). Porous melt flow can be buoyancy-driven (Solano, Jackson, Sparks, Blundy, & Annen, 2012) or stress-driven via deformation (Hasalová, Schulmann, et al., 2008a).

There are several styles of porous melt flow where intragranular melt movement is diffusive (passive movement along grain boundaries), channelized (restricted within channels, commonly physically or chemically armoured), and/or reactive (reactions at grain boundaries between melt and mineral) (Stuart, Meek, Daczko, Piazolo, & Huang, 2018).

Porous melt flow styles have been largely invoked for melt movement in the mantle, where the associated chemical and mineralogical changes are well documented (Dijkstra, Barth, Drury, Mason, & Vissers, 2003; Kelemen, Dick, & Quick, 1992; Kelemen, Shimizu, & Salters, 1995; Rampone, Piccardo, Vannucci, Bottazzi, & Zanetti, 1994). In particular, formation of dunite channels (Aharonov, Whitehead, Kelemen, & Spiegelman, 1995; Braun & Kelemen, 2002; Kelemen et al., 1995; Spiegelman, Kelemen, & Aharonov, 2001) and harzburgite channels (Kelemen et al., 1992) in the mantle have been attributed to formation via porous melt flow, and subsequent metasomatism. The increased interest in porous melt flow processes in the mantle occurred where classic mantle geochemical signatures were not found, for example where geochemical compositions of mafic rocks were too enriched or depleted in major, trace or rare earth elements to be derived from primitive mantle. In many cases, melt-rock interactions induced metasomatism of the mantle via coupled dissolution-precipitation replacement reactions, all facilitated by porous melt flow.

More recently, porous melt flow has also been suggested for melt movement in the Earth's oceanic crust (Collier & Kelemen, 2010; Coogan, Saunders, Kempton, & Norry, 2000; Lissenberg, MacLeod, Howard, & Godard, 2013; Lissenberg & Dick, 2008; Rampone et al., 2016; Sanfilippo et al., 2015) and arc crust (Cashman, Sparks, & Blundy, 2017; Daczko, Piazolo, Meek, Stuart, & Elliott, 2016; Smith, 2014; Stuart, Daczko, & Piazolo, 2017; Stuart, Meek, et al., 2018; Stuart, Piazolo, & Daczko, 2016; Wu et al., 2018; Závada et al., 2018). Many of these studies have focussed primarily on the geochemical signatures found in lower arc and oceanic crustal sequences, which could not be explained by typical crystal fractionation from primitive magmas. Due to the relatively low viscosity contrasts of melt and rock within the lower arc crust, porous melt flow within the crust is believed to require deformation to proceed efficiently (Hasalová, Schulmann, et al., 2008a). However, porous melt flow has been shown to occur in both static and dynamic environments (Stuart et al., 2017; Stuart, Meek, et al., 2018; Stuart et al., 2016).

The aim of this contribution is to develop an in-depth understanding of the mechanisms involved in deformation-assisted, channelized reactive porous melt flow in lower arc crust and therefore identify its expression from the field to the micron scale. We examine a hornblende-rich body (i.e. hornblendite), commonly found in mafic crust (e.g. Daczko, Emami, Allibone, & Turnbull, 2012; Debari, Kay, & Kay, 1987; Fanka et al., 2016; Pál-Molnár et al., 2015) typically characterised as igneous cumulates. We show in this study, a hornblendite which exhibits features that preclude an igneous cumulate origin and instead presents evidence for formation via reactive porous melt flow through lower crustal gabbroic gneiss, accommodated by shear zone deformation and chemical armouring, that results in grain-scale coupled dissolution-precipitation replacement reactions. Within this contribution, we refer to the host rock as gabbroic gneiss, and the hornblende-rich body or hornblendite as the reaction product. Our results suggest that porous melt flow may play a larger role within lower arc crustal environments as well as early earth crustal formation (Sizova, Gerya, Stüwe, & Brown, 2015) and invites further work in identifying cryptic mass transfer zones and their expression.

REGIONAL GEOLOGY AND PREVIOUS WORK

We chose the field area due to its exceptional exposure, absence of post-melt flux overprint and frequency of such melt transfer zones from the cm to 10s m scale (e.g. Daczko et al. 2016, Stuart et al. 2018). The field area lies in the Pembroke Valley located in New Zealand's South Island (Fig. 1a) and represents one of the few exposed lower crustal sections of magmatic arc crust that preserves nearly exclusively deep arc conditions (Allibone et al., 2009; Blattner, 1991; Chapman, Clarke, & Daczko, 2016; Chapman, Clarke, Piazolo, & Daczko, 2017; Clarke, Fitzherbert, Milan, Daczko, & Degeling, 2010; Clarke, Klepeis, & Daczko, 2000; De Paoli, Clarke, & Daczko, 2012; Milan, Daczko, & Clarke, 2017; Milan, Daczko, Clarke, & Allibone, 2016; Mortimer et al., 1999). Within the Pembroke Valley, the so-called Pembroke Granulite is exposed. This granulite is part of the Median Batholith, comprising Carboniferous to Early Cretaceous magmatic arc rocks which were rapidly exhumed with little to no tectonometamorphic overprint (Blattner, 1976; Bradshaw, 1990; Clarke et al., 2000; Daczko, Clarke, & Klepeis, 2001a; Daczko, Klepeis, & Clarke, 2001b).

The Pembroke Granulite is a low-strain gabbroic gneiss (GG) with pervasive foliation, exhibiting a two-pyroxene-pargasite-plagioclase assemblage. Its igneous protolith was emplaced at 139–129 Ma (Hollis, Clarke, Klepeis, Daczko, & Ireland, 2003) or 163–150 Ma, (Stowell, Tulloch, Zuluaga, & Koenig, 2010).

The gabbroic igneous assemblage (enstatite, diopside, pargasite, plagioclase, ilmenite) was variably recrystallised during D_1, forming a strongly aligned, steeply dipping S_1 gneissosity striking NE. The granulite facies gneissosity is defined by alignment of pargasite and preferred orientation of recrystallized clusters of enstatite, diopside and plagioclase (Clarke et al., 2000). Similar syn-deformational metamorphic assemblages in nearby orthogneiss bodies formed at lower crustal conditions of 850ºC and <11 kbar (Daczko & Halpin, 2009). A recent study showed that the S_1 assemblage records a post-tectonic partial hydration during an early episode of incipient melt-assisted diffuse porous melt flow (Stuart, Meek, et al., 2018). During melt-rock interaction with an externally-derived, hydrous melt, the S_1 assemblage became partially hydrated post-D_1, to pargasite, quartz, clinozoisite and plagioclase at 630–710ºC and 8.8–12.4 kbar (Stuart et al., 2017; Stuart et al., 2016).

A second tectonometamorphic event (D_2) is characterized by brittle fracturing associated with sub-vertical felsic dykes cutting the S_1 gneissosity. Two orthogonal rectilinear dyke orientations dominate (Daczko, Clarke, et al., 2001a). Within a halo of 1-10 cm associated with the crosscutting dykes, melt-rock dehydration reactions partially replace the S_1 and early porous melt flow assemblages, and transformed it nearly isochemically into garnet granulite (Blattner, 1976; Bradshaw, 1989a; Daczko, Clarke, et al., 2001a; Smith, Piazolo, Daczko, & Evans, 2015). Termed garnet reaction zones (GRZ) in previous literature, the melt-rock reactions occur as a result of volatile scavenging by the anhydrous trondhjemitic melt during melt flux through the dykes (Clarke et al., 2005). Melt-rock interaction conditions occurred at 720–890ºC and 12–16 kbar (Daczko & Halpin, 2009). D_3 deforms both D_1 and D_2 fabrics at granulite facies (676 ± 34ºC and 14 ± 1.26 kbar) forming narrow (cm–m) variably dipping shear zones (Daczko, Klepeis, et al., 2001b).

Besides the Pembroke Granulite of gabbroic composition, granulite with dioritic and ultramafic compositions have been reported, and the observed compositional range was attributed to variations in igneous protolith (Clarke et al., 2000; Daczko, Clarke, et al., 2001). However, recently the occurrence of these dioritic and ultramafic bodies have been reinterpreted to be indicative for moderate to extensive melt-rock interactions between gabbroic gneiss protoliths and externally-derived reactive melts (Daczko et al., 2016; Stuart, Meek, et al., 2018). The lenses of ultramafic composition, termed hornblende-rich bodies in this study, cut D_1-D_2, and is considered to be associated with either D_3 deformation or forms as the last deformational event (D_4) within the Pembroke Granulite geological history prior to rapid uplift.

The geochemical signatures of the hornblende-rich body are discussed in another contribution and there is referred to as Style 4 (Stuart, Meek, et al. (2018). Whole rock REE patterns of the hornblende-rich body show a middle-REE hump typical of hornblende cumulates. Amphibole in the hornblende-rich body is predominantly pargasite, with REE distributions increasing from

La to Eu (0.04-2.6 times chrondrite, a positive Eu anomaly, then flat yet enriched (up to 6 times chrondrite) MREE and HREE patterns. Clinozoisite (pistacite content between 12 and 18) is found across all four porous melt flow styles within the Pembroke Granulite (Stuart et al., 2018) with little appreciable changes in composition. REE patterns are typical of igneous clinozoisite, where LREE are significantly enriched, followed by a flat and steep HREE trend (Stuart et al., 2018).

METHODS

Petrographic analysis was completed using a petrographic microscope in combination with the Virtual Petrographic Microscope (Tetley & Daczko, 2014) on polished thin (30 μm) sections made from blocks cut from representative samples. Mineral identification and microstructural relationships of the samples were determined using plane-polarised light microscopy and back-scatter electron (BSE) imaging. BSE imaging was performed on a Hitachi Desktop Scanning Electron microscope (SEM; OptoFab node of the Australian National Fabrication Facility, Macquarie University) run at low vacuum, 15 kV accelerating voltage and working distances between 9–11 mm. Higher resolution imaging (15–30 kV, 10 nA beam current and working distances between 10–12.5 mm) was completed using a Carl Zeiss IVO scanning electron microscope (Macquarie University Geoanalytical (MQGA)).

Electron back-scatter diffraction (EBSD) analysis was performed on selected samples using the Carl Zeiss IVO SEM (MQGA) at 20kV and 8.0 nA. Patterns were acquired with HKL NordlysNano high sensitivity EBSD detector and indexed using AzTec analysis software (Oxford Instruments). Samples were tilted at 70º and analysed at working distances between 11–24.5 mm. Step sizes ranged between 1–8 μm dependent on the spatial resolution required. Channel 5 software was used for post-processing and all maps were cleaned using a "standard" noise reduction following Prior, Wheeler, Peruzzo, Spiess, and Storey (2002), Bestmann and

Prior (2003) and Piazolo, Bestmann, Prior, and Spiers (2006). Grain boundaries and subgrain boundaries have misorientations larger than 2° and less than 10º, respectively. Pole figures are equal area projections. EBSD mapping and analysis is applied to all samples used in the study, for consistency throughout the project.

Whole rock major element compositions were determined by XRF at the Mark Wainwright Analytical Centre, University of New South Wales (UNSW), Australia. Samples were processed using a PW2400 WDXRF Spectrometer. Whole rock powders were crushed using a hydraulic press with tungsten carbide plates and then reduced to a fine powder in a tungsten carbide barrel and ring Tema mill. Powders were fused into glass discs using lithium borate at 1050ºC for major element analysis. Loss on ignition (LOI) was established by heating the samples to 1050ºC for 1 hour.

FIELD RELATIONSHIPS

We report results from several occurrences of hornblende-rich rocks that cut the two-pyroxene-pargasite components of the Pembroke Granulite (Figure 1a inset). Samples are taken from two main sites. Site 1 exhibits a 30–40 m wide hornblende-rich body extending for >250 m along strike across the Pembroke Valley (Figure 1a). The outcrop was mapped in detail (Fig. 1b) and shows that the body consists of an irregularly shaped hornblende-rich rock body, surrounded by a 2–7 m wide zone characterized by hydration of the otherwise largely anhydrous host gabbroic gneiss. In the following, the latter zone is termed the transition zone. Samples were extracted in-situ from the main hornblende-rich body of this study (site 1), and are supplemented with samples from a smaller, 0.5–20 cm thick, continuous band of hornblendite that occurs over a distance of more than 100 m (site 2, Fig. 1c, d).

Characteristics of the host two-pyroxene-pargasite gabbroic gneiss (GG)

In outcrop, the host rock type is a two-pyroxene-pargasite gneiss (Pembroke Granulite). It has a pervasive S_1 gneissosity defined by preferred orientation of coarse-grained and partially recrystallized igneous pyroxenes (enstatite, diopside), pargasitic hornblende and plagioclase (Fig. 2a, 2a inset, 2b, 2c, Table 1). Recrystallization is most pronounced in plagioclase. A common feature of the Pembroke Granulite is the occurrence of wide-spread rectilinear dyking (Fig. 2a). This dyking pattern is easily discernible in the field as dykes are always associated with 2–5 cm wide garnet reaction zones (GRZ) either side of the dykes (Fig. 2a, Table 1). The S_1 gneissic foliation is often partially preserved both in the gabbroic gneiss (Fig. 2b) and GRZ (Fig. 2c) (Fig. 2a-c).

Characteristics of the hornblende-rich bodies (H)

The hornblende-rich bodies strike at an angle to the gneissosity of the gabbroic gneiss and GRZ. The hornblende-rich bodies are typically composed of >50–90% hornblende (pargasitic) with minor minerals (clinozoisite, garnet and plagioclase). Three main rock types of the hornblende-rich bodies are distinguished: (i) clinozoisite-hornblendite (H(Cz-Hbl)) (>10 area % clinozoisite), (ii) hornblendite sensu stricto (H(Hbl)) (<10 area % clinozoisite) and (iii) pegmatite (P) (Fig. 1b). In addition, throughout the hornblende-rich body, cm-wide bands of garnetite (± rare plagioclase and hornblende) are present within all rock types (Table 1).

Clinozoisite-hornblendite (H(Cz-Hbl)) is the dominant rock type, yet in places is cut by anastomosing zones of hornblendite (Fig. 1b., 3a). Hornblende is dark-coloured and coarse-grained (up to 5mm width) in both clinozoisite-hornblendite and hornblendite (Fig. 3a). Clinozoisite grains are pale green and elongate (up to 5mm length) with aspect ratios of 2–5. They are found randomly oriented (Fig. 3a), except close the hornblendite body–transition zone boundary where they are mapped to delineate high-strain zones based on their shape preferred orientation subparallel to the boundaries of the hornblendite body (Fig. 1b). Plagioclase (< 5 area %) occurs as an interstitial mineral in both rock types (Fig. 3a).

Pegmatite bodies are found throughout the Site 1 hornblendite; these vary in size from small pegmatitic domains (cm-scale) to extensive pegmatite bodies (m-scale) (Fig. 1b, 3b, 3b inset). Pegmatite consists of elongate, euhedral crystals of hornblende (up to 10 cm length), tabular plagioclase (up to 10 cm length) and euhedral garnet (1–10 cm) (Fig. 3b, 3b inset). Pegmatite is hosted within both clinozoisite-hornblendite and hornblendite. Pegmatite bodies are generally irregularly shaped on all scales (cm-m scale) (Fig. 3b) and may completely embody and surround areas of the hornblende-rich body (Fig. 3b, 3b inset).

Garnet is the main constituent of distinct bands of garnetite, named garnetite stringers (Fig. 3c). The garnetite stringers are thin (<2–5cm wide), medium to coarse grained, and dominated by ~90–95 area % garnet, with minor fine-grained plagioclase and hornblende (Fig. 3c, Table 1). Garnetite stringers are continuous over several meters to tens of meters, found within both clinozoisite-hornblendite and hornblendite (Fig. 3a, c, d, Fig. 4f) and as fragments in the pegmatitic bodies (Fig. 3b).

In some areas, single, isolated euhedral (1–10 cm) garnet grains are seen in the hornblende-rich body (Fig. 3c, Table 1). These garnets are dark red in colour, notably inclusion free and may be surrounded by a thin 1–5 mm rim of plagioclase aggregates (Fig. 3d, 3d inset). These isolated garnets may also occur within or in close proximity to pegmatite bodies (Fig. 3b) and are found frequently close to the boundary of these rock units to the transition zone (Fig. 3d).

Characteristics of the transition zone (TZ)

The transition zone forms an irregular halo either side of the hornblende-rich body, ranging between 2–7 m in width for Site 1 (Fig. 1b) and more than 5 m for Site 2. This zone is defined as a portion of host two-pyroxene-pargasite gneiss (i.e. Pembroke Granulite), where the mineral assemblages of both the gneiss and GRZ (sensu stricto) have been hydrated. The transition zone is formed by a hornblende-feldspar gneiss where, instead of pyroxene clusters, elongate clusters of hornblende pseudomorph the variably transposed S_1 gneissosity (Fig. 2a, 10a, Table 1). The prevalent GRZ markers from the two pyroxene-pargasite gneiss are found to be progressively mineralogically modified (Fig. 4a, Fig. 5c, d). The typical 5 cm wide GRZ (sensu stricto) becomes thinner, reduced to ~1–2 cm widths (Fig. 4a, 5a, b), and is surrounded by either feldspar or hornblende (Fig. 4a, Fig. 5c,d). Individual GRZ from the host rock (two-pyroxene-pargasite gneiss) can be traced continuously through the transition zone and directly into the hornblende-rich body (Fig. 5a, b) where they become the garnetite stringers, discussed above (Fig. 3a–d). Furthermore, the S_1 gneissic foliation present in the host rock can be traced into the foliated transition zone. However, the two-pyroxene assemblage has been hydrated to pargasite (Table 1).

There are several distinct, angular to rounded "islands" of transition zone within the hornblende-rich body ranging in scale from 30 cm–8 m length (Fig. 1b, 3e, f). They are generally lozenge-shaped, low-strain bodies exhibiting as the rest of the transition zone with a distinct pargasite defined gneissic foliation, inferred to be a transposed, pseudomorphed and hydrated S1 fabric (Fig. 3e, f).

Contact Relationships

The boundaries between the transition zone and hornblende-rich body are irregular, but sharp, and easily discernible due to the pronounced colour change and complete loss of the gneissic foliation seen within the transition zone but not in the hornblende-rich body (Fig. 4b, c, Table 1). The boundary is characterized by finger-like protrusions of hornblende-rich body into the transition zone which gradually thin to a sharp point (Fig. 4b, c, d, Fig. 5a). These sharp points are spatially associated with the mineralogically modified GRZ in the transition zone (Fig. 5a).

These modified GRZ are continuous to garnetite stringers in the hornblende-rich body. While the highly irregular boundary is a common feature, some contact boundaries are regular and lack hornblende-rich body protrusions (Fig. 1b, Fig. 4d, Fig. 5b). In these cases, GRZ are sub-parallel to parallel to the boundary between transition zone and the hornblende-rich body (Fig. 5a, b).

The boundary between the host gneiss and transition zone is less well-defined in the field. It is characterized by two main features; a distinct change in mineralogy of the GRZ and loss of pyroxene (as described above) resulting in hornblende being the main mafic mineral. Different to the boundary between hornblende-rich body and the transition zone, the gneissic S_1 foliation is continuous across the boundary (Fig. 4c, d).

Strain variations

The fact that GRZ have a well-defined rectilinear pattern within the host rock and can be continuously traced into the transition zone and hornblende-rich body, allows their use as reaction and strain markers utilizing the orientation and relative angles of different GRZ sets. Within the transition zone and hornblende-rich body, modified GRZ are variably deformed (Fig. 4a, 5a,b). Here, the intensity of deformation generally increases towards and within the hornblende-rich body (Fig. 5a, b). Strain intensity is observed to be independent from discernible mineralogical differences (i.e. garnet-rich stringers surrounded by felsic or mafic minerals). At both the northern and southern sides of the hornblende-rich body, modified GRZ are deflected when entering the transition zone, suggesting apparent sinistral displacement (Fig. 1b, 5a, b). This deflection in the transition zone is accompanied by deflection and transposition of the S_1 foliation (Fig. 5a). Modified GRZ continue into the hornblende-rich body, now garnetite stringers, where they are variably deformed (Fig. 5a). Within the hornblende-rich body, the observed angles between different garnetite stringers show that strain levels are highly variable. Some domains show low-strain, where garnetite stringers preserve near-rectilinear patterns, with angles similar to those found in GRZ throughout the Pembroke Valley (compare Figs. 2 & 5e). Open to tight folds of garnetite stringers form symmetric (Fig. 5f) and asymmetric folds (Fig. 5g) and indicate moderate to high-strain. Sheath folds occur in zones interpreted as high-strain zones close to the boundary to the transition zone (Fig. 5h). In these zones, clinozoisite shows a distinct shape preferred orientation (Fig. 5b).

WHOLE ROCK CHEMISTRY

Whole rock XRF chemistry of major element compositions of the host gabbroic gneiss, transition zone and the hornblende-rich body (separated into sub-units as clinozoisite-hornblendite and hornblendite) shows that the host gneiss and the rocks within the transition zone have very similar whole rock chemistry in terms of SiO_2, MgO, Fe_2O_3 and Na_2O except a slight increase (from 0.4 to 0.9) in LOI in the transition zone rocks (Fig. 6). This stands in stark contrast to the clinozoisite-hornblendite and hornblendite rock types which exhibit a marked decrease in silica content and Na_2O, and an increase in MgO and Fe_2O_3 (Fig. 6). Further to this, LOI values of the hornblende-rich body are increased further to 1.4–2.0. Further details regarding whole rock REE patterns are provided by Stuart, Meek, et al. (2018).

DETAILED PETROGRAPHY AND QUANTITATIVE ORIENTATION ANALYSIS OF THE MAIN ROCK TYPES

Clinozoisite-hornblendite

The clinozoisite-hornblendite rock is dominated by green hornblende (up to ~80 area %) and clinozoisite (up to ~50 area %) (Fig. 7a, Table 1). Hornblende grains are subhedral to anhedral and locally display a narrow Gaussian grain size distribution, with a grain size range of 0.5–5 mm and an average grain size around 3 mm. Hornblende is inclusion-free and has no shape preferred orientation (Fig. 7a, b). Clinozoisite grains are elongate, euhedral crystals with rounded tips, and have a narrow Gaussian grain size distribution between 1–5 mm in length and peak size 2.5 mm. Crystals are no more than 1–3 mm wide with aspect ratios between 2 and 3. Clinozoisite grains regularly have inclusions of rounded green hornblende (<0.05 mm) (Fig. 7a). Some clinozoisite grains have more complex, equidimensional multiphase inclusions of hornblende, plagioclase, clinochlore and K-feldspar (Fig. 7c, d, e). Clinozoisite is commonly randomly orientated (Fig. 3a, c). However, they can also have a distinct shape preferred orientation in higher strain areas (Fig. 5a, b, Fig. 7a).

Plagioclase is a minor mineral (< 5 area %) of the clinozoisite hornblendite. It is found only as small grains along grain boundaries of hornblende, clinozoisite and garnet (in the case of the garnetite stringers) and at triple junctions of the latter (Fig. 7a, b, e, f, h, i). They do not display the rectangular shape typical for euhedral, igneous plagioclase crystals. Instead, they are elongate grains, with pointed ends, with some grains exhibiting low apparent dihedral angles of between <10º—<60° (Fig. 7b, e, f, g, h) giving them an interstitial appearance. There is an abundance of low dihedral angles <60°, however, of particular interest are several very low apparent dihedral angles <10° (Fig. 7f, g). Measurements of apparent low dihedral angles are made using BSE images via ImageJ. A histogram of the apparent angles shows a relatively even spread of angles between <10°—<60° (Fig. S1). Plagioclase grains display no shape preferred orientation. EBSD analyses show that small plagioclase grains at clinozoisite and/or hornblende boundaries are often connected in 3D, even if not connected in 2D (Fig. 7b inset). This is shown by plagioclase grains showing the same crystallographic orientation including twin relationships across several small nearby plagioclase grains (Fig. 7b inset).

Multiphase inclusions within clinozoisite show that clinozoisite hosting the inclusion and the clinozoisite "within" the inclusions have the same crystallographic orientation (Fig. 7e). Within a single inclusion, hornblende and clinochlore each exhibit, per phase, the same crystallographic orientation (Fig. 7 e). Plagioclase also has similar orientations including some twin orientations (Fig. 7e). Within these multiphase inclusions, mineral grain boundaries are interlobate–amoeboid, rarely displaying crystal faces (Fig. 7c-e) where hornblende is seen to have the largest grain size with other minerals being finer grained (Fig. 7d–e).

In some cases, plagioclase grains are associated with near circular domains made of a mixture of biotite, hornblende, garnet, apatite and oxides (rutile or ilmenite) (Fig. 7h). Also, in these cases, EBSD analyses confirm the plagioclase to be a single grain, i.e., with the same crystallographic orientation including twin boundaries (Fig. 7i).

Hornblendite

The hornblendite is dominated by green hornblende (~95 area %) (Table 1). Subhedral to anhedral hornblende displays a bimodal grain size distribution (large grains up to 5 mm length/width, with smaller grains >0.5–2 mm) with near equant grains (Fig. 8a). Hornblende is inclusion free and has no shape preferred orientation (Fig. 8a). By definition, less than 10 area % of clinozoisite is present (Table 1). Plagioclase is a minor constituent (<5 area %), present only as distinct highly elongate grains along grain boundaries of hornblende, between 1–5 mm length (Fig. 8a, b). They similarly have pointed tips and commonly display low apparent dihedral angles of <10º (Fig. 8a, b). Plagioclase is generally inclusion-free. However, some plagioclase grains situated at hornblende triple junctions (~650 μm wide) have inclusions of biotite, garnet and oxides (e.g. rutile) (Fig. 8b, c). In this case, plagioclase exhibits highly irregular boundaries, with several boundaries ending in pointed ends, some with very low apparent dihedral angles of <10º (Fig. 8b–d). Euhedral to subhedral, tabular biotite inclusions (50–450 μm length) are randomly orientated within the plagioclase cluster and are found both within the plagioclase as well as in contact with the surrounding hornblende (Fig. 8b). Within these clusters, garnet (50–150μm) is generally rounded with cuspate–lobate grain edges and completely enclosed by plagioclase (Fig. 8b). All garnet grains within the plagioclase cluster have the same crystallographic orientation (Fig. 8d and inset). However, plagioclase shows two main orientations ignoring their respective twins (Fig. 8d).

Garnetite stringers

Garnetite stringers are present within both clinozoisite-hornblendite and hornblendite; they exhibit the same characteristics in both rock types (Fig. 7a, 8a). Garnetite stringers are comprised predominantly of medium–coarse grained (100–700 μm), inclusion-free garnet (~95 area %) (Fig. 9a–e, Table 1). Garnet grains have highly irregular shapes, interlocking amoeboidal grain boundaries and no shape preferred orientation. Garnet crystallographic orientation data highlight the lack of any crystallographic preferred orientation; e.g. grain orientations have a wide spread (Fig. 9d, pole figure, all data). Within individual grains, sub-grain boundaries (>5–10º misorientation) and irregular intra-grain lattice distortions are seen (Fig. 9d,e, pole figure, blue grain). Both features show a distinct lack of clear dispersion patterns, i.e., small circle dispersions seen in pole figures (Fig. 9d).

Plagioclase (<5 area %, Table 1) within garnetite stringers is present as elongate grains along garnet grain boundaries, with pointed ends, and some ending in very low apparent dihedral angles of <10º (Fig. 9a–c). Plagioclase is sometimes interlocked with hornblende (Fig. 9a–c). Plagioclase around surrounding hornblende grains shows crystallographic continuity (Fig. 9b). Hornblende may exhibit subhedral to anhedral shapes (Fig. 9c).

Transition zone hornblende-feldspar gneiss and its contact with hornblende-rich body rock types

Both hornblendite and clinozoisite-hornblendite are in contact with the transition zone (Figs 1b, 5a–b). This section focusses on the details of the boundary between the transition zone gneiss and hornblendite units. Hornblende grains found at the boundary of the two rock types are finer grained (up to 2mm length) than those found in the hornblende-rich rock types and the gabbroic gneiss (compare Fig. 2b & Fig. 7a, 8a, 10a). At the boundary, hornblende within the hornblendite is inclusion-free and exhibits a weak shape-preferred orientation, similar to the foliation in the transition zone hornblende-feldspar gneiss. As typical for the transition zone, this hornblende-feldspar gneiss is very similar to the two pyroxene-pargasite gneiss (Fig. 2b) where elongate clusters of hornblende define the gneissosity within a plagioclase-rich matrix, except hornblende has replaced the two-pyroxene assemblage (Fig. 2a, 10a, Table 1).

The boundary between the two rock types is abrupt, with a mineralogical change at a single-grain-scale (Fig. 10a–c). Plagioclase mode decreases from 45 area% in the hornblende-feldspar gneiss of the transition zone to <5 area% in the hornblendite, while hornblende mode increases from 45 area% to >95 area% (Fig. 10a, Table 1). Directly at the boundary, hornblende in the transition zone and within the hornblende-rich body are similar in orientation and size. However, while plagioclase is present as both large (mm sized) porphyroclasts and small, recrystallized grains within the transition zone, at the boundary it is seen as small grains or "partially replaced remnants" surrounded by hornblende (Fig. 10b).

The immediate contact boundary is irregular at the grain-scale. Here, hornblende and plagioclase grain boundaries are highly irregular exhibiting a strongly corroded, cuspate-lobate nature (Fig. 10a–c, 10b inset). Plagioclase has a bimodal grain size distribution (Fig. 10b, inset). Larger plagioclase grains (>100 μm) resemble those seen in the transition zone hornblende-feldspar gneiss where they exhibit tapered and bent twins (Fig. 10b). Where plagioclase and hornblende are in direct contact, clusters of smaller grains of plagioclase are present (< 50–100 μm) (Fig. 10b inset). They show no internal deformation features or crystallographic preferred orientation (Fig. 10b). Hornblende also shows a bimodal grain size distribution where large grains are up to 2mm in length and smaller grains of hornblende (<50–100 μm) occur in clusters (Fig. 10c). Plagioclase remnants found within hornblende grains exhibit crystallographic orientations continuous with plagioclase adjacent to the hornblende grain (arrow on Fig. 10b). Small hornblende grains are seen between plagioclase grains and in rare cases along twin planes (Fig. 10c). Interestingly, hornblende is commonly seen to occur between grain boundaries of large plagioclase grains (Fig. 10b–e), irrespective of twin plane orientation. In rare instances, hornblende is found along sub-grain boundaries of plagioclase (Fig. 10e).

DISCUSSION

The Pembroke Granulite, Fiordland, provides an exceptionally well exposed window into the lower arc crust, and therefore has been extensively investigated in earlier literature in the light of its tectonometamorphic evolution (Blattner, 1976; Bradshaw, 1989a; Bradshaw, 1989b; Clarke, Daczko, Klepeis, & Rushmer, 2005; Clarke et al., 2000; Daczko, Clarke, et al., 2001; Daczko, Clarke, & Klepeis, 2002; Daczko, Klepeis, et al., 2001; Gardner, Piazolo, & Daczko, 2016; Klepeis, Clarke, & Rushmer, 2003; Mortimer et al., 1999; Schröter et al., 2004; Smith et al., 2015; Stevenson, Daczko, Clarke, Pearson, & Klepeis, 2005; Stuart et al., 2017). Different to previous studies, this study focusses on the hornblende-rich bodies, which in earlier studies have not been considered in detail and been referred to as 'ultramafic pods or bodies' (Clarke et al., 2000; Daczko, Clarke, et al., 2001). We discuss below evidence for the protolith of the hornblende-rich body, and likely formation processes. Hornblendites have been shown to form from fractional crystallisation (Jagoutz, Müntener, Schmidt, & Burg, 2011) as well as hydration of gabbroic gneiss igneous protolith (Wade, Dyck, Palin, Moore, & Smye, 2017). We show that while there are several 'igneous-like' characteristics suggesting a potential cumulate fractionation origin (part 1), other features preclude this interpretation (part 2), and instead point to a melt-rock interaction process.

Hornblende-rich body: a late tectonic "igneous body" hosted in an actively deforming zone that cuts a metamorphic terrain

We discuss features of the hornblende-rich body typical for an 'igneous-like' body post-dating the main regional tectonometamorphic events. This interpretation is based on three key observations:

I. Field relationships suggest that the hornblendite postdates the two earliest tectonometamorphic events in the Pembroke Granulite. The boundaries of the hornblendite cross-cuts the regional S_1 foliation, D_2 formation of garnet reaction zones (GRZ) and D_3 shear zones.
II. The hornblende-rich body has an igneous character in terms of cumulate-like mineralogy (up to ~50-95% hornblende), presence of pegmatites that are spatially linked to the hornblende-rich body (Fig. 1b, Fig. 3b) and microstructures indicative of the former presence of melt.
III. The whole-rock geochemistry of the hornblende-rich body is distinct from the gabbroic gneiss exhibiting characteristics typical for igneous ultramafic lenses (Fig. 6) (Clarke et al., 2005; Daczko, Klepeis, et al., 2001).

The hornblende-rich body is present within the regional gabbroic gneiss which records three early deformation events ($D_{1\text{–}3}$). D_1 is a high temperature tectonometamorphic event, resulted in solid-state crystal plasticity (Fig. 10b, e, Smith et al., 2015). D_2 is recorded by rectilinear dyking, where anhydrous melt infiltrates through a dyke network and reacts with host gneiss, transforming the adjacent rock to garnet granulite in distinct 2–5 cm garnet reaction zones (GRZ) (Blattner, 1976; Clarke et al., 2005; Daczko, Clarke, et al., 2001; Schröter et al., 2004). In contrast, the hornblende-rich body commonly lacks a well-developed foliation, except in high-strain areas, where moderate to strongly developed shape preferred orientations can be seen in both hornblende and clinozoisite (Fig. 1b, Fig.8a, Fig. 10a).

Field relationships suggest that the hornblende-rich body is hosted within a post-D_2 deformation zone. This is illustrated by systematic bending of the S_1 gneissosity and the pre-existing D_2 GRZ into the hornblendite body (particularly those oriented perpendicular to the hornblende-rich body–host boundary (Fig. 1b, 5a,b) indicating a component of sinistral shearing (Fig. 1b, 5 a, b). The relative timing of the hornblende-rich body is either syn-deformational with respect to D_3 shear zones, or is post-D_3 deformation (Stuart, Meek, et al., 2018).

Furthermore, within the hornblende-rich body, strain variation is apparent: (i) anastomosing near pure hornblendite areas are seen within a predominantly hornblende-clinozoisite rock and are oriented subparallel to the transition zone – hornblende-rich body boundary (Fig. 1b) and (ii) simple folding and stretching to sheath folding of modified GRZ are common within the hornblendite-rich body (Fig. 5e-h). The consistency of displacement structures at the contact between the host gneiss and the hornblende-rich body, and parallelism of structures within the body with body boundaries suggests an external stress regime causing sinistral shearing associated with hornblende-rich body formation.

The locally near-chaotic folding suggests that some volume loss occurred, however, the continuity of GRZ from outside to within the hornblende-rich body precludes high volume losses which would result in disjunct collapse structures (Bons, Druguet, Castaño, & Elburg, 2008) or avalanches of instabilities with hydrofractures (Bons et al., 2004).

Microstructures related to the *former* presence of melt in a rock have been widely characterised and a set of criteria agreed upon in the literature. They have been characterised extensively in migmatites (Hasalová, Schulmann, et al., 2008a; Holness & Sawyer, 2008; Vernon, 2011) and cumulate rocks (Holness, Cheadle, & McKenzie, 2005; Holness, Clemens, & Vernon, 2018). Key microstructures include: 1) interstitial, often monomineralic films present along grain boundaries (e.g. hornblende and/or garnet, Figs 7b, h, Fig. 8b, Fig. 9a), 2) low dihedral angles (<60°) of minerals representing pseudomorphs of former melt in equilibrium with solid minerals (e.g. plagioclase, Figs 7b, f, g, h, Fig. 8b, Fig. 9a), 3) irregularly shaped pockets (cuspate-lobate or embayed boundaries) commonly containing blocky, euhedral minerals inferred to have grown from the melt (e.g. Fig. 7h, i, Fig. 8b–d), 4) neoblasts growing into indentations (embayments) of melt-filled boundaries (e.g. plagioclase neoblasts interpreted to represent pseudomorphed interconnected 3D melt networks (Fig. 7b, inset, Fig. 9b)), and 5) mineral growths with orientations sub-perpendicular or perpendicular to neighbouring minerals (Hasalová, Schulmann, et al., 2008a; Holness, 2006; Holness & Sawyer, 2008; Marchildon & Brown, 2002; Sawyer, 1999; Sawyer, 2001; Vernon, 2011). Although these textures are used to identify the former presence of a melt at some point in the rocks' geological history, they are rarely linked to melt-rock interaction and/or melt movement through a host rock. Consequently, linking microstructures indicative of the former presence of melt to the mechanisms of pervasive melt migration and porous melt flow replacement reactions is desirable.

The dihedral angle of a melt between two solid minerals has a primary control on the permeability of the rock and hence, controls the connectivity of melt distribution and enhances melt migration (Holness, 2006; Vernon, 2011). Therefore, melt-solid-solid dihedral angles of 60º or less have been shown to allow interconnected melt networks to flow in geological systems (Holness, 2006), as opposed to isolated melt-filled pores (>60º) which stagnates melt and prevents flow. During cooling, melt will solidify into these pore networks, and pseudomorph the pore space used during melt movement (Hasalová, Schulmann, et al., 2008a; Holness, 2006; Sawyer, 2001; Vernon, 2011). In the studied system, apparent dihedral angles are as low as 10º (Fig. 7b, f, g, h, 8b, 9a).

When melt-solid-solid dihedral angles approach zero, grain boundary melt films are pseudomorphed by highly elongate grains of the interstitial phase along grain boundaries (Rosenberg & Riller, 2000). Hence, films of primarily plagioclase (Fig. 7b, f, g, h, 8b, 9a, and in rarer instances, hornblende, Fig. 7h, 9a-c) along grain boundaries of hornblende, clinozoisite and garnet, are interpreted to indicate pseudomorphs of grain boundary melt networks. Pore spaces bound by fewer than four surrounding solid grains will typically be pseudomorphed by single grains (i.e. plagioclase in this example; Hasalová et al 2008). However, as pore size increases between solid grains, so does the ability of polymineralic aggregates to crystallize. Multiphase crystal aggregates (biotite, garnet, apatite, rutile in this study) hosted within single plagioclase grains are interpreted to indicate late stage crystallization of melt-filled pores during cooling (Fig. 7h, i, Fig. 8b-d) (Holness & Sawyer, 2008; Sawyer, 2001). As plagioclase crystallizes (generally 1–2 main grains depending on the pore size), other minerals are able to crystallize from the melt composition, leading to multiphase crystal aggregates that replace former melt pockets (Holness & Sawyer, 2008).

Discontinuous films of interstitial plagioclase along grain boundaries, are sometimes shown to be connected in 3D (due to their single, consistent twin set orientations) even when not connected in 2D (Fig. 7b, inset, Fig. 9b). These results are consistent with melt crystallizing and pseudomorphing an interconnected melt porosity (Holness & Sawyer, 2008) forming an interstitial texture. Low nucleation rates are also likely to play a role (Vernon, 2004).

The very coarse grained pegmatitic patches are only seen within the hornblende-rich body (Fig. 1b, Fig. 3b). These are characterized by typical igneous textures with plagioclase as an interstitial mineral (Fig. 3b). This, along with the fact that these pegmatitic bodies have very diffuse, irregular boundaries and comprise the same mineral assemblage as the rest of the hornblende-rich body suggests that the pegmatite is part of the hornblende-rich body. Consequently, these pegmatites are likely to represent the accumulation and final precipitation of the melt associated with the formation of the hornblende-rich body, as late-stage low pressure zones. In summary, the abundant microstructures indicative of the former presence of melt and pegmatitic bodies within the hornblende-rich body are consistent with an igneous origin.

Hornblende-rich body: A product of melt-rock interaction involving melt-mediated reactions

Field relationships indicate that the hornblende-rich body cannot have intruded as a dyke or hydrofracture into the pre-existing two-pyroxene-pargasite gneiss as there is no definitive or clear structural break between the different rock types. Furthermore, the continuity and modification of previously existing GRZ from the host gneiss through the transition zone into the hornblende-rich body necessitates the hornblende-rich body to be a product of extreme modification of the host gneiss (Daczko et al., 2016). This modification must have occurred *in situ* to enable the observed structural continuity (Fig. 4a, b, 5c, d). Porphyroblastic growth of euhedral garnet (some with surrounding feldspar rich rims, see Fig. 3d inset) are common within the transition zone, particularly close to the contact of the hornblende-rich body, as well as within the hornblende-rich body and pegmatite domains (Fig. 3b-d). These large euhedral garnets point to the growth of minerals in the presence of a melt (Stuart et al., 2017). The leucosome material closely associated with these euhedral garnets (Fig. 3d inset) are consistent with felsic pseudomorphs after melt (Stuart et al. 2017).

Microstructures within the hornblende-rich body show unequivocally that it formerly contained melt and that the microstructural development is closely related to reactive melt-rock interactions and melt crystallisation. This is particularly clear at the contact boundary between the transition zone and the hornblende-rich body where microstructures are consistent with plagioclase being dissolved and replaced by hornblende (Fig. 10b–e). Boundaries between plagioclase and hornblende are highly irregular. Orientation mapping shows the older, remnant plagioclase of the gabbroic gneiss retains deformation twinning, while newly grown hornblende shows no evidence of high-grade solid-state deformation (Fig. 10b). As strained crystal lattices and deformation twinning are typical in the host gneiss and absent within the hornblendite body, the hornblendite is post-tectonic (post-S_1). The remnants of old plagioclase within newly formed hornblende grains at the hornblendite–transition zone boundary are interpreted to reflect a disequilibrium texture, where the plagioclase was unstable and dissolved to produce hornblende. We suggest that this disequilibrium was induced by interaction with an externally-derived reactive melt. At the contact between a reactive melt and the pre-existing two-pyroxene-pargasite gneiss, coupled dissolution-precipitation replacement reactions occurred (Putnis, 2009). In such reactions, the phase that is chemically unstable (i.e. undersaturated within the fluid/melt) is dissolved into the fluid/melt and the phase that is oversaturated with respect to the fluid grows (Spruzeniece, Piazolo, Daczko, Kilburn, & Putnis, 2017). If these processes are coupled, the new phase replaces the volume occupied by the dissolving phase (Putnis, 2009). If this process occurs in an open fluid system, the original material will show a marked decrease in the abundance of the unstable phase and an increase in the stable phase. In our example, modal percentages (Table 1) of plagioclase and hornblende of the host gneiss (45, 20% respectively, with 25% pyroxenes present), moderately change in the transition zone (45, 45% respectively, pyroxenes absent) before dramatically changing in the hornblende-rich body (<5, up to 95% respectively), as a result of melt-mediated replacement reactions within an open system. Interestingly, plagioclase twin boundaries appear to have no influence on melt infiltration or reaction, as we do not see any preferred plagioclase dissolution and hornblende crystallization along these twins (Fig. 10a-e).

Within the hornblende-rich body, hornblende grains exhibit subhedral to anhedral grain shapes, with some euhedral crystal faces; whereas, clinozoisite exhibits euhedral grain boundaries with poikilitic structures, similar to a weakly ophitic texture caused by low nucleation rates (Vernon, 2004). Neither mineral exhibits compositional zoning. We interpret these features may indicate rapid growth within a confined space after nucleation, or sparse nucleation within a melt-present system. Garnet grains within garnetite stringers exhibit unusual amoeboid grain shapes, which we also interpret to occur due to melt-mediated reactions (Figs 9d, e). We infer that garnetite stringers are where melt has reacted with and intensely modified pre-existing GRZ. In this case, the melt dissolves plagioclase and pyroxene from GRZ and replaces these with garnet, forming amoeboid garnet grain shapes. Of note are the frequent subgrain boundaries and lattice distortions within the garnet (Fig. 9d, e). Further to this, garnetite stringers are corroded and warped by melt-rock reactions, associated strain and deformation, and are therefore significantly thinner within the hornblende-rich body compared to the width of the original GRZ (Figs 2a versus Figs 5e-h). In summary, we suggest that these features are a product of rapid replacement reactions which are found to be similar to the microstructures formed during experimental fluid-mediated replacement reaction in salts (Spruzeniece, Piazolo, & Maynard-Casely, 2017).

Our microstructural observations at the boundary between the hornblende-rich body and the transition zone demonstrate that the host gneiss reacted with the melt, in the following reaction involving reactive flow of an externally-derived melt: Cpx + Opx + Pl + $melt_1 \rightarrow$ Hbl ± Cz ± Grt + $melt_2$. Relevant melt-rock reaction experiments are lacking and are needed to explore these processes. However, igneous phase equilibria experiments investigating the stabilities of ferromagnesian silicates (pyroxene, hornblende, clinozoisite, biotite) and plagioclase (+ quartz) within H_2O-rich granodioritic melt (8–11 wt.% H_2O), indicate that these minerals are co-stable within *T*= ~675–720 ºC at 8 kbar (Naney, 1983), possibly pointing toward an intermediate composition melt being involved in the formation of the clinozoisite-bearing hornblendite rocks. Other experiments that investigated phase equilibria for gabbroic and andesitic melts (with up to ~5 wt. % H_2O) found that the addition of water depresses the solidus and liquidus of the system and increases the stability of hydrous minerals (Green 1982). This is consistent with our interpretation that melt-mediated replacement reactions can occur between rocks with little chemical variation (i.e. hydrous gabbroic melt reacting with gabbroic rock may form hornblendite at high-T conditions near the liquidus of the hydrous melt).

Hornblende in this study is pargasite amphibole (Stuart, Meek, et al., 2018) which is known to be a high P-T amphibole (Niida & Green, 1999). The abundance of clinozoisite within the hornblende-rich body, with euhedral crystal faces and abundant pargasite hornblende inclusions suggests they crystallised together (Figure 7a). Although clinozoisite is found regularly in lower temperature epidote-amphibolite facies, numerous studies, both experimental (Johnston & Wyllie, 1988; Naney, 1983) and in natural samples (Evans & Vance, 1987; Zen & Hammarstrom, 1984) have shown that it can also form magmatically at higher pressures and temperatures (Schmidt & Poli, 2004). Textural criteria are established to infer magmatic epidote: (i) euhedral to subhedral grain shapes with clear grain boundaries and (ii) mineral associations with primary hornblende (Pandit, Panigrahi, & Moriyama, 2014). Primary magmatic clinozoisite has also been identified petrographically in ultramafic rocks where euhedral grains consist of inclusions of hornblende (and minor garnet), as is similar to our case (Bazylev, Ledneva, Kononkova, & Ishiwatari, 2013). Geochemically, pistacite (Ps) content is used to attempt and distinguish magmatic from metamorphic epidote. However, this has not proven to be a useful indicator due to indistinguishable data (Schmidt & Poli, 2004). In contrast, rare earth element patterns have been shown to be distinct for igneous versus metamorphic epidote and the clinozoisite grains in the hornblende-rich body of this study have rare earth element patterns consistent with them being of igneous origin (Stuart et al., 2018b).

The composition of the fluxing melt was likely a hydrous granodioritic to gabbroic magma. This conclusion is consistent with the mineralogical assemblage found in the hornblende-rich body (hornblende and clinozoisite) and the melt pockets (plagioclase-hosted with crystallizations of biotite, garnet, hornblende, apatite and oxides) as well as the mineral assemblage of plagioclase, hornblende, garnet and clinozoisite observed in the pegmatitic bodies. Our results also agree with experimental data (i.e. Naney, 1983; Green, 1982). A granodioritic to gabbroic magma is also more probable as mafic melts have lower viscosities (Lesher & Spera, 2015; Shaw, 1972). The presence of co-existing garnet and biotite within some melt pockets may indicate either simultaneous crystallization from a possible granodioritic composition or may show a late-stage back-reaction of garnet and melt to biotite (Fig. 8b–e).

To summarize, we suggest that the influx of an externally-derived, hydrous silicate melt of varying granodioritic to gabbroic composition, has induced melt-mediated coupled dissolution-precipitation replacement reactions, replacing an anhydrous gabbroic gneiss and GRZ. In this scenario, where the reacting melt infiltrates at the grain-scale, pyroxene and plagioclase react with the melt and are dissolved, preferentially along grain and sub-grain boundaries (Fig. 10b, e, Fig. 11). At the same time, hornblende with or without clinozoisite and garnet precipitate *in situ* (Fig. 10c, e, Fig. 11) forming a coupled dissolution-precipitation reaction (Putnis, 2009). Hornblende growth is seen along grain and sub-grain boundaries of plagioclase (Fig. 10c, e) (Levine, Mosher, & Rahl, 2016) resulting in remnants or "islands" of plagioclase within an undeformed hornblende grain (Fig. 10b, c). The observation of finer grained hornblende at the transition zone-hornblendite boundary suggests there is high reaction affinity and a strong driving force to nucleate hornblende in place of plagioclase. In contrast to relatively rapid heating, as seen in contact aureoles, high reaction affinity and overstepping reactions can also be produced by extreme chemical disequilibrium (Roselle, Baumgartner, & Chapman, 1997). Small plagioclase grains are also found, suggesting that locally the melt composition changes and/or connectivity to the open system is hindered, resulting in local re-precipitation of fine-grained plagioclase (Fig. 10b, Fig. 11). Similarly, garnet grows within the pre-existing GRZ.

Here plagioclase is dissolved but garnet grows as pre-existing garnet likely acts as easy nucleation sites. Hence, local kinetics must govern their growth.

Evidence of both high-variance hornblende-only and hornblende-clinozoisite-rich areas suggests melt-mediated metasomatism (Korzhinskiĭ, 1959) involving variable melt compositions, which occurred due to an evolving melt composition from progressive melt-rock reactions and/or a change in temperature regimes. Clinozoisite-rich areas are likely later in the progression of evolving melt compositions or P-T changes, where clinozoisite nucleates within predominantly hornblende-rich body, replacing hornblende with euhedral grains. This is a more likely scenario than forming epitaxial clinozoisite grains on hornblende.

Deformation-assisted, channelized reactive porous melt flow: a mechanism of mass transfer within the lower arc crust

Successful melt-mediated replacement reactions require an efficient process for melt migration, otherwise the reaction will stall (Jonas, Müller, Dohmen, Baumgartner, & Putlitz, 2015). In other words, if the reactive melt cannot access the reactive host rock, no reaction can take place. We propose that the mechanism facilitating melt migration and open system behaviour involves pervasive melt movement along grain boundaries during deformation in a shear zone. During melt-present deformation, melt infiltrates along grain boundaries and within triple junctions, forming an interconnected, highly permeable network of melt movement (Scott & Stevenson, 1986; Turcotte & Ahern, 1978). This mechanism of porous melt flow is commonly invoked for lower strain formation of mantle melt conduits, as well as transporting melt through focused channels within the mantle (Dijkstra et al., 2003; Kelemen et al., 1995). In these scenarios, the viscosity and density contrast between host rock and migrating melt are larger compared to within the Earth's crust. Our study suggests that a similar mechanism is an important process of pervasive melt migration through generally anhydrous lower arc crust but requires accompanying deformation to proceed. For porous melt flow to be effective, there must be a driving force for melt migration and pathways, i.e. porosity that does not close as a result of the melt-rock reaction and a permeable interconnected network. Porosity and permeability are likely to be maintained during ongoing deformation.

Movement of melt via porous flow can be, in principle, buoyancy-driven (Solano et al., 2012), or stress-driven via deformation (Hasalová, Schulmann, et al., 2008a). In situations where deformation-assisted melt percolation occurs (e.g. in shear zones), porosity is dynamically produced (Fusseis, Regenauer-Lieb, Liu, Hough, & De Carlo, 2009; Hasalová, Schulmann, et al., 2008a). If the migrating melt is mafic and has a high water content, porous melt flow is easier to achieve, as elevated water contents lower melt viscosity by several orders of magnitude (Richet, Lejeune, Holtz, & Roux, 1996; Shaw, 1972; Stuart et al., 2016). At the same time, hydrous melt would result also in a decrease of the dihedral angle between minerals and melt allowing better grain-scale connectivity (Fujii, Osamura, & Takahashi, 1986). Still, the density contrast between the host rock and melt may not be sufficiently large to allow buoyancy-driven porous melt flow in the crust. Hence, the necessary additional factor enabling significant porous melt flow in the lower arc crust is deformation (Hasalová, Schulmann, et al., 2008a). In our case, the fact that the reactive melt must have been mafic–intermediate, hydrous and occurred in a shear zone, supports the interpretation that a combination of buoyancy and deformation-driven porous melt flow facilitated melt migration. Here, sinistral shearing (as seen by the deflection of GRZ into the transition zone and hornblende-rich body in the field, Fig. 1b, Fig. 5a, b) has resulted in dynamic porosity generation and therefore assisted porous melt flow through the system; this allowed reactions to occur geologically fast.

We suggest that the melt-rock reaction occurred dominantly at grain boundaries. In the case of a coupled dissolution-precipitation replacement reaction, dissolution of the unstable phases will create porosity and therefore permeability, further allowing the migrating melt to move through the constantly evolving grain boundary networks (Kelemen et al., 1995). Similar to scenarios advocated for e.g. dunite channel production in the mantle (Braun & Kelemen, 2002), minerals in equilibrium with the melt will not only nucleate and grow, but importantly dissolution of minerals creates space, allowing the process to occur *in situ*. The dissolution-precipitation process increases permeability and helps drive a continuous melt flux through the system. Volume changes involved in melt-rock interactions may additionally create space or increase melt fluid pressure, resulting in fracturing and further reaction (Jamtveit, Putnis, & Malthe-Sørenssen, 2009).

The model of melt-mediated dissolution-precipitation replacement reactions presented here, closely resembles field and experimental studies on mantle rocks. As such, several studies have characterized the formation of dunite (Ol) (Kelemen et al., 1995; Morgan & Liang, 2003; Pec, Holtzman, Zimmerman, & Kohlstedt, 2017), lherzolite (Ol + Opx + Cpx) (Morgan & Liang, 2005) and harzburgite (Ol + Opx) (Kelemen et al., 1992) via reaction with a silica over- or under-saturated melt. Typically, the composition of the melt that migrates through a host rock, the composition of the host rock (i.e. mantle peridotite), and P-T conditions dictates which minerals will dissolve and precipitate. For mantle conditions, this process is thought to be initiated by geochemical melt compositions (basalt or fractionated versions thereof) significantly different to the host rock compositions (peridotite, dunite, harzburgite). The vast geochemical differences can easily initiate chemical disequilibrium, as there are large differences in the relative solubility of the dissolving versus precipitating minerals in the melt that will drive melt-mediated replacement reactions. Interestingly, field studies of these processes in mantle rocks (Kelemen et al., 1995) show the same angular remnants or “islands” of un-reacted host material within the reacted zones as we observe in our field example of lower crust (Fig, 1b, Fig. 4e, f).

In summary, we propose the development of the melt flux zone to occur in the following way, (i) an influx of an externally-derived, hydrous silicate melt (of approximate gabbroic to granodioritic composition) into the anhydrous gabbroic gneiss occurs during high-strain deformation, (ii) melt migrates via porous melt flow along grain boundaries, (iii) the melt is reactive with the host gneiss and dissolves pyroxene and plagioclase, starting at grain or sub-grain boundaries (Levine et al., 2016) (Fig. 11), (iv) this increases porosity and permeability, enhancing large volumes of melt flow through the system, (v) hornblende (± clinozoisite, garnet) replaces pyroxene/plagioclase *in situ* via a coupled dissolution-precipitation replacement-reaction (Fig. 11), which is dependent on the stability regime of minerals involved and melt composition, (vi) the reaction occurs preferentially at grain and subgrain boundaries where transport is fastest until the mineral is completely replaced; this results in cuspate-lobate and embayed reaction fronts at the melt-grain interface, (vii) the growing minerals may form some igneous-like crystal facets, (viii) as the melt-rock interactions mature, the melt flow is focused into a channel-like structure which become chemically armoured where the migrating melt is no longer in contact with the host gabbroic gneiss. This results in the arrest of further melt-rock interaction at the observed structural level and the unreactive flow of the melt through the armoured channel (Daczko et al., 2016).

Geochemical studies comparing the "host" and "reacted" rock types formed from crustal porous melt flow have shown little to no chemical differences between the identified rock types, which has been suggested as evidence for low melt fractions (Hasalová, Schulmann, et al., 2008a; Stuart, Meek, et al., 2018; Stuart et al., 2016). In our example, the hornblende-rich body is interpreted to have formed by extensive reactive modification of the enclosing anhydrous gabbroic gneiss, surrounded by a transition zone 'halo', where pyroxene grains have reacted to hornblende (Daczko et al., 2016). We interpret the hornblendite to indicate high time-integrated volumes of melt flux and melt-rock interactions that have run to completion, due to the lack of any precursor rock found within main hornblende-rich body, with the exception of isolated remnants of the transition zone (Stuart, Meek, et al., 2018). These remnants, along with the surrounding transition zone, are characterized by a lack of pyroxene and the growth of peritectic garnet with leucosome, and these features indicate lower melt-rock interactions compared with the main hornblende-rich body.

Our study shows that the presence of hornblende-rich rocks does not necessitate a cumulate origin. Instead, hornblendite rocks may be produced by melt transfer and melt-mediated replacement reactions. Furthermore, reaction softening by growth of rheologically "soft" minerals (in our case, hornblende and clinozoisite) (Brodie & Rutter, 1985) is shown by garnetite stringers deflecting around transition zone remnants in the hornblende-rich body (see Fig. 4f) and alignment of clinozoisite in folded garnetite stringers (Fig. 5b). However, once melt flux stops, remnant melt will crystalize and locally cause rheological hardening (Prakash et al., 2018). Hence, softening may be intermittent and upon cooling and crystallisation of the melt, the zone is likely to be preserved as subsequent deformation will localize in rheologically softer domains (Diener & Fagereng, 2014; Gardner, Piazolo, Evans, & Daczko, 2017). The recognition that hornblende-rich bodies and their surrounding (e.g. hydrated neighbouring rocks) may be formed by melt-rock interaction has important implications for the interpretation of geochronological data derived from these rocks. For example, Langone et al. (2018) showed that melt-rock (and fluid-rock) interactions affect zircon geochronology by altering mineral isotopic and REE-element compositions and the ages derived from such rocks.

Nonetheless, our model is applicable to mafic bodies hosted within lower arc crustal environments (ancient and present) as we invite the re-evaluation of igneous-like bodies that may have formed by a similar mechanism to the hornblende-rich body in this study. We provide field and microstructural criterion that can be used to identify the origin of such bodies. Geochemical signatures are provided in a separate contribution (Stuart, Meek, et al., 2018). We suggest this mechanism is applicable to hot, mafic crust that may be fluxed by hydrous melts of almost similar composition, where melt moves via porous melt flow. We show that hydrous versus anhydrous compositions can provide enough disequilibrium to initiate grain-scale melt-rock reactions.

How to recognise zones of former melt flux in lower crustal terranes

In conclusion, we propose the following features of field, microstructural, and whole rock chemical characteristics as indicative for mass melt transfer within lower arc crust. Field observations show a body with a high variance assemblage with igneous features within a metamorphic rock. However, different to a dyke, the body does not crosscut structural features but instead results in significant yet progressive changes in mineral assemblage and bulk composition. Specifically, field signatures of such melt flux include (i) finger-like apophyses or highly irregular contact boundaries, formed via melt-mediated, coupled dissolution-precipitation replacement reactions and associated localized porosity generation, (ii) the occurrence of a hydrated halo (i.e. transition zone), triggering partial replacement and localized partial melting evidenced by growth of peritectic minerals i.e. porphyroblastic euhedral garnet surrounded by leucosome, (iii) modification of pre-existing features (if available, such as previous dykes), in mineralogy, shape, orientation, etc., and the loss or addition of minerals while preserving their structural continuity, (iv) presence of pegmatite components that shows evidence of syn-deformational emplacement, (v) remnant bodies of less reacted sections of original host rock within the hornblende-rich body. Whole rock chemistry of the zone of former melt flux is distinct from that of host rocks, even when structural continuity can be seen between the rock types. Within the zones of former mass transfer, microstructures indicating the former presence of melt include (i) elongate films along grain boundaries, (ii) melt pockets (iii) low dihedral angles <60º, as well as 3D melt network connectivity seen from orientation mapping indicates the ability of the melt to flow within a system. Reaction microstructures including (i) instability fronts between reacting minerals, where heavily cuspate-lobate or amoeboid grain boundaries show evidence of disequilibrium, allowing dissolution of unstable minerals to occur, and precipitation or replacement by stable minerals, (ii) lattice distortion with no systematic orientation (i.e. stress, strain, deformation) indicating melt-mediated replacement reactions, and (iii) irregular grain boundaries and "remnants" of old grains within new grains, indicate melt-rock interactions. These signatures, along with high melt fractions (as seen in this case) have allowed the reaction to run to completion. As the underlying process of melt-mediated replacement reactions occurs exceptionally fast and in a confined space, crystal shapes will not be euhedral, but have some subhedral to anhedral crystal faces, and limited compositional zoning develops if the geochemistry of the fluxing melt remains relatively similar throughout the event.

In this present work, we concentrate on an example of deformation-assisted migration of a hydrous mafic melt through relatively anhydrous mafic arc crust. However, similar microstructures and reaction textures should be expected in more felsic, granitic orogenic lower crustal systems of melt transfer, though reaction products and interstitial minerals will be different. We suggest that in regions where melt networks are pre-existing and/or where deformation forms pressure gradients and facilitates permeable connection with a melt source, pervasive melt flow could proceed. As mineral stabilities are dependent on the externally derived melt composition and the host rock composition, as well as the P-T conditions of the system, we suggest that biotite will be an important product of hydration crystallisation reactions in felsic systems. The interstitial minerals are also likely to involve quartz and/or K-feldspar, in addition to plagioclase. The interested reader is pointed to research focussing on the rheology of felsic granitic systems with interstitial melt flow (Hasalová, Janoušek, Schulmann, Štípská, & Erban, 2008b; Hasalová, Schulmann, et al., 2008a; Hasalová, Štípská, et al., 2008c; Schulmann et al., 2008; Štípská et al., 2019; Závada, Schulmann, Konopásek, Ulrich, & Lexa, 2007; Závada et al., 2018).

Understanding this process allows for better understanding of lower crustal rheology; where deformation assisted, channelized reactive melt flow produces a transient rheologically soft unit, where post-crystallization and post-melt flux hardening allows preservation of mass melt transfer conduits and their delicate microstructures.

ACKNOWLEDGEMENTS

ARC Future Fellowship (FT110100070) to SP and Discovery Project funding (DP120102060) to SP and NRD provided financial support to conduct this research. We thank the Department of Conservation, New Zealand for permission to visit and sample localities in the Fiordland National Park. Johann Diener, Brendan Dyck and an anonymous reviewer are thanked for careful reviews. We also thank Michael Brown for editorial handling. This is contribution XXX from the ARC Centre of Excellence for Core to Crust Fluid Systems (www.ccfs.mq.edu.au) and XXX from the GEMOC Key Centre (www.gemoc.mq.edu.au).

REFERENCES

Aharonov, E., Whitehead, J., Kelemen, P., & Spiegelman, M. (1995). Channeling instability of upwelling melt in the mantle. *Journal of Geophysical Research: Solid Earth, 100*(B10), 20433-20450.

Allibone, A., Jongens, R., Turnbull, I., Milan, L., Daczko, N. R., DePaoli, M., & Tulloch, A. (2009). Plutonic rocks of western Fiordland, New Zealand: field relations, geochemistry, correlation, and nomenclature. *New Zealand Journal of Geology and Geophysics, 52*(4), 379-415.

Bazylev, B. A., Ledneva, G. V., Kononkova, N. N., & Ishiwatari, A. (2013). High-pressure ultramafics in the lower crustal rocks of the Pekul'ney complex, central Chukchi Peninsula. 1. Petrography and mineralogy. *Petrology, 21*(3), 221-248. doi:10.1134/s0869591113030028

Beach, A., & Fyfe, W. S. (1972). Fluid transport and shear zones at Scourie, Sutherland: Evidence of overthrusting? *Contributions to Mineralogy and Petrology, 36*(3), 175-180. doi:10.1007/bf00371429

Bercovici, D. (2003). The generation of plate tectonics from mantle convection. *Earth and Planetary Science Letters, 205*(3), 107-121. doi:https://doi.org/10.1016/S0012-821X(02)01009-9

Bestmann, M., & Prior, D. J. (2003). Intragranular dynamic recrystallization in naturally deformed calcite marble: diffusion accommodated grain boundary sliding as a result of subgrain rotation recrystallization. *Journal of Structural Geology, 25*(10), 1597-1613. doi:https://doi.org/10.1016/S0191-8141(03)00006-3

Blattner, P. (1976). Replacement of hornblende by garnet in granulite facies assemblages near Milford Sound, New Zealand. *Contributions to Mineralogy and Petrology, 55*(2), 181-190. doi:10.1007/bf00372225

Blattner, P. (1991). The north Fiordland transcurrent convergence. *New Zealand Journal of Geology and Geophysics, 34*(4), 533-542.

Bons, P. D., Arnold, J., Elburg, M. A., Kalda, J., Soesoo, A., & van Milligen, B. P. (2004). Melt extraction and accumulation from partially molten rocks. *Lithos, 78*(1-2), 25-42.

Bons, P. D., Druguet, E., Castaño, L.-M., & Elburg, M. A. (2008). Finding what is now not there anymore: Recognizing missing fluid and magma volumes. *Geology, 36*(11), 851-854. doi:10.1130/G24984A.1

Bradshaw, J. (1989a). Early Cretaceous Vein-Related Garnet Granulite in Fiordland, Southwest New Zealand: A Case for Infiltration of Mantle-Derived-Rich Fluids. *The Journal of Geology, 97*(6), 697-717.

Bradshaw, J. (1989b). Origin and metamorphic history of an Early Cretaceous polybaric granulite terrain, Fiordland, southwest New Zealand. *Contributions to Mineralogy and Petrology, 103*(3), 346-360.

Bradshaw, J. (1990). Geology of crystalline rocks of northern Fiordland: details of the granulite facies Western Fiordland Orthogneiss and associated rock units. *New Zealand Journal of Geology and Geophysics, 33*(3), 465-484.

Braun, M. G., & Kelemen, P. B. (2002). Dunite distribution in the Oman ophiolite: implications for melt flux through porous dunite conduits. *Geochemistry, Geophysics, Geosystems, 3*(11), 1-21.

Brodie, K., & Rutter, E. (1985). On the relationship between deformation and metamorphism, with special reference to the behavior of basic rocks *Metamorphic reactions* (pp. 138-179): Springer.

Brown, M. (2010). Melting of the continental crust during orogenesis: the thermal, rheological, and compositional consequences of melt transport from lower to upper continental crustThis article is one of a selection of papers published in this Special Issue on the the theme Lithoprobe—parameters, processes, and the evolution of a continent. *Canadian Journal of Earth Sciences, 47*(5), 655-694. doi:10.1139/E09-057

Carter, K. E., & Dworkin, S. I. (1990). Channelized fluid flow through shear zones during fluid-enhanced dynamic recrystallization, Northern Apennines, Italy. *Geology, 18*(8), 720-723. doi:10.1130/0091-7613(1990)018<0720:cfftsz>2.3.co;2

Cartwright, I., & Barnicoat, A. C. (2003). Geochemical and stable isotope resetting in shear zones from Täschalp: constraints on fluid flow during exhumation in the Western Alps. *Journal of Metamorphic Geology, 21*(2), 143-161. doi:10.1046/j.1525-1314.2003.00423.x

Cashman, K. V., Sparks, R. S. J., & Blundy, J. D. (2017). Vertically extensive and unstable magmatic systems: A unified view of igneous processes. *Science, 355*(6331). doi:10.1126/science.aag3055

Chapman, T., Clarke, G., & Daczko, N. (2016). Crustal differentiation in a thickened arc—evaluating depth dependences. *Journal of Petrology, 57*(3), 595-620.

Chapman, T., Clarke, G., Piazolo, S., & Daczko, N. (2017). Evaluating the importance of metamorphism in the foundering of continental crust. *Scientific Reports, 7*(1), 13039.

Clarke, G., Daczko, N., Klepeis, K., & Rushmer, T. (2005). Roles for fluid and/or melt advection in forming high-P mafic migmatites, Fiordland, New Zealand. *Journal of Metamorphic Geology, 23*(7), 557-567.

Clarke, G., Fitzherbert, J., Milan, L., Daczko, N., & Degeling, H. (2010). Anti-clockwise P–T paths in the lower crust: an example from a kyanite-bearing regional aureole, George Sound, New Zealand. *Journal of Metamorphic Geology, 28*(1), 77-96.

Clarke, G., Klepeis, K., & Daczko, N. (2000). Cretaceous high-P granulites at Milford Sound, New Zealand: metamorphic history and emplacement in a convergent margin setting. *Journal of Metamorphic Geology, 18*(4), 359-374.

Collier, M. L., & Kelemen, P. B. (2010). The Case for Reactive Crystallization at Mid-Ocean Ridges. *Journal of Petrology, 51*(9), 1913-1940. doi:10.1093/petrology/egq043

Coogan, L., Saunders, A., Kempton, P., & Norry, M. (2000). Evidence from oceanic gabbros for porous melt migration within a crystal mush beneath the Mid-Atlantic Ridge. *Geochemistry, Geophysics, Geosystems, 1*(9).

Daczko, N., Clarke, G., & Klepeis, K. (2001). Transformation of two-pyroxene hornblende granulite to garnet granulite involving simultaneous melting and fracturing of the lower crust, Fiordland, New Zealand. *Journal of Metamorphic Geology, 19*(5), 549-562.

Daczko, N., Clarke, G., & Klepeis, K. (2002). Kyanite-paragonite-bearing assemblages, northern Fiordland, New Zealand: rapid cooling of the lower crustal root to a Cretaceous magmatic arc. *Journal of Metamorphic Geology, 20*(9), 887-902.

Daczko, N., Emami, S., Allibone, A., & Turnbull, I. (2012). Petrogenesis and geochemical characterisation of ultramafic cumulate rocks from Hawes Head, Fiordland, New Zealand. *New Zealand Journal of Geology and Geophysics, 55*(4), 361-374.

Daczko, N., & Halpin, J. A. (2009). Evidence for melt migration enhancing recrystallization of metastable assemblages in mafic lower crust, Fiordland, New Zealand. *Journal of Metamorphic Geology, 27*(2), 167-185.

Daczko, N., Klepeis, K., & Clarke, G. (2001). Evidence of Early Cretaceous collisional-style orogenesis in northern Fiordland, New Zealand and its effects on the evolution of the lower crust. *Journal of Structural Geology, 23*(4), 693-713.

Daczko, N., Piazolo, S., Meek, U., Stuart, C. A., & Elliott, V. (2016). Hornblendite delineates zones of mass transfer through the lower crust. *Scientific Reports, 6*, 31369. doi:10.1038/srep31369

De Paoli, M., Clarke, G. L., & Daczko, N. (2012). Mineral equilibria modeling of the granulite–eclogite transition: effects of whole-rock composition on metamorphic facies type-assemblages. *Journal of Petrology, 53*(5), 949-970.

Debari, S., Kay, S. M., & Kay, R. (1987). Ultramafic xenoliths from Adagdak volcano, Adak, Aleutian Islands, Alaska: deformed igneous cumulates from the Moho of an island arc. *The Journal of Geology, 95*(3), 329-341.

Diener, J. F., & Fagereng, Å. (2014). The influence of melting and melt drainage on crustal rheology during orogenesis. *Journal of Geophysical Research: Solid Earth, 119*(8), 6193-6210.

Dijkstra, A. H., Barth, M. G., Drury, M. R., Mason, P. R. D., & Vissers, R. L. M. (2003). Diffuse porous melt flow and melt-rock reaction in the mantle lithosphere at a slow-spreading ridge: A structural petrology and LA-ICP-MS study of the Othris Peridotite Massif (Greece). *Geochemistry, Geophysics, Geosystems, 4*(8), n/a-n/a. doi:10.1029/2001GC000278

Evans, B. W., & Vance, J. A. (1987). Epidote phenocrysts in dacitic dikes, Boulder County, Colorado. *Contributions to Mineralogy and Petrology, 96*(2), 178-185.

Fanka, A., Tsunogae, T., Daorerk, V., Tsutsumi, Y., Takamura, Y., Endo, T., & Sutthirat, C. (2016). Petrochemistry and mineral chemistry of Late Permian hornblendite and hornblende gabbro from the Wang Nam Khiao area, Nakhon Ratchasima, Thailand: Indication of Palaeo-Tethyan subduction. *Journal of Asian Earth Sciences, 130*, 239-255.

Fujii, N., Osamura, K., & Takahashi, E. (1986). Effect of water saturation on the distribution of partial melt in the Olivine-Pyroxene-Plagioclase System. *Journal of Geophysical Research: Solid Earth, 91*(B9), 9253-9259.

Fusseis, F., Regenauer-Lieb, K., Liu, J., Hough, R. M., & De Carlo, F. (2009). Creep cavitation can establish a dynamic granular fluid pump in ductile shear zones. *Nature, 459*, 974. doi:10.1038/nature08051

https://www.nature.com/articles/nature08051 - supplementary-information

Gardner, R. L., Piazolo, S., & Daczko, N. R. (2016). Shape of pinch and swell structures as a viscosity indicator: Application to lower crustal polyphase rocks. *Journal of Structural Geology, 88*, 32-45. doi:https://doi.org/10.1016/j.jsg.2016.04.012

Gardner, R. L., Piazolo, S., Evans, L., & Daczko, N. R. (2017). Patterns of strain localization in heterogeneous, polycrystalline rocks – a numerical perspective. *Earth and Planetary Science Letters, 463*, 253-265. doi:https://doi.org/10.1016/j.epsl.2017.01.039

Gurnis, M. (1988). Large-scale mantle convection and the aggregation and dispersal of supercontinents. *332*, 695. doi:10.1038/332695a0

Hasalová, P, Janoušek, V., Schulmann, K., Štípská, P., & Erban, V. (2008). From orthogneiss to migmatite: geochemical assessment of the melt infiltration model in the Gföhl Unit (Moldanubian Zone, Bohemian Massif). *Lithos, 102*(3-4), 508-537.

Hasalová, P, Schulmann, K., Lexa, O., Štípská, P., Hrouda, F., Ulrich, S., . . . Týcová, P. (2008). Origin of migmatites by deformation-enhanced melt infiltration of orthogneiss: a new model based on quantitative microstructural analysis. *Journal of Metamorphic Geology, 26*(1), 29-53. doi:10.1111/j.1525-1314.2007.00743.x

Hasalová, P, Štípská, P., Powell, R., Schulmann, K., Janoušek, V., & Lexa, O. (2008). Transforming mylonitic metagranite by open-system interactions during melt flow. *Journal of Metamorphic Geology, 26*(1), 55-80.

Hollis, J. A., Clarke, G., Klepeis, K., Daczko, N., & Ireland, T. (2003). Geochronology and geochemistry of high-pressure granulites of the Arthur River Complex, Fiordland, New Zealand: Cretaceous magmatism and metamorphism on the palaeo-Pacific Margin. *Journal of Metamorphic Geology, 21*(3), 299-313.

Holness, M. (2006). Melt–Solid Dihedral Angles of Common Minerals in Natural Rocks. *Journal of Petrology, 47*(4), 791-800. doi:10.1093/petrology/egi094

Holness, M., Cheadle, M. J., & McKenzie, D. A. N. (2005). On the Use of Changes in Dihedral Angle to Decode Late-stage Textural Evolution in Cumulates. *Journal of Petrology, 46*(8), 1565-1583. doi:10.1093/petrology/egi026

Holness, M., Clemens, J. D., & Vernon, R. H. (2018). How deceptive are microstructures in granitic rocks? Answers from integrated physical theory, phase equilibrium, and direct observations. *Contributions to Mineralogy and Petrology, 173*(8), 62. doi:10.1007/s00410-018-1488-8

Holness, M., & Sawyer, E. (2008). On the Pseudomorphing of Melt-filled Pores During the Crystallization of Migmatites. *Journal of Petrology, 49*(7), 1343-1363. doi:10.1093/petrology/egn028

Jagoutz, O., Müntener, O., Schmidt, M. W., & Burg, J.-P. (2011). The roles of flux- and decompression melting and their respective fractionation lines for continental crust formation: Evidence from the Kohistan arc. *Earth and Planetary Science Letters, 303*(1), 25-36. doi:https://doi.org/10.1016/j.epsl.2010.12.017

Jamtveit, B., Putnis, C. V., & Malthe-Sørenssen, A. (2009). Reaction induced fracturing during replacement processes. *Contributions to Mineralogy and Petrology, 157*(1), 127-133.

Johnston, A. D., & Wyllie, P. J. (1988). Constraints on the origin of Archean trondhjemites based on phase relationships of Nuk Gneiss with H 2 O at 15 kbar. *Contributions to Mineralogy and Petrology, 100*(1), 35-46.

Jonas, L., Müller, T., Dohmen, R., Baumgartner, L., & Putlitz, B. (2015). Transport-controlled hydrothermal replacement of calcite by Mg-carbonates. *Geology, 43*(9), 779-782.

Kelemen, P. B., Dick, H. J. B., & Quick, J. E. (1992). Formation of harzburgite by pervasive melt/rock reaction in the upper mantle. *Nature, 358*(6388), 635-641.

Kelemen, P. B., Shimizu, N., & Salters, V. J. M. (1995). Extraction of mid-ocean-ridge basalt from the upwelling mantle by focused flow of melt in dunite channels. *Nature, 375*(6534), 747-753.

Klepeis, K. A., Clarke, G. L., & Rushmer, T. (2003). Magma transport and coupling between deformation and magmatism in the continental lithosphere. *GSA TODAY, 13*(1), 4-11.

Korzhinskiĭ, D. S. (1959). *Physicochemical basis of the analysis of the paragenesis of minerals*: Consultants Bureau.

Langone, A., Zanetti, A., Daczko, N., Piazolo, S., Tiepolo, M., & Mazzucchelli, M. (2018). Zircon U–Pb dating of a lower crustal shear zone: a case study from the northern sector of the Ivrea-Verbano Zone (Val Cannobina, Italy). *Tectonics*.

Lee, A. L., Torvela, T., Lloyd, G. E., & Walker, A. M. (2018). Melt organisation and strain partitioning in the lower crust. *Journal of Structural Geology, 113*, 188-199.

Lesher, C. E., & Spera, F. J. (2015). Thermodynamic and transport properties of silicate melts and magma *The Encyclopedia of Volcanoes (Second Edition)* (pp. 113-141): Elsevier.

Levine, J. S. F., Mosher, S., & Rahl, J. M. (2016). The role of subgrain boundaries in partial melting. *Journal of Structural Geology, 89*, 181-196. doi:https://doi.org/10.1016/j.jsg.2016.06.006

Lissenberg, C. J., MacLeod, C. J., Howard, K. A., & Godard, M. (2013). Pervasive reactive melt migration through fast-spreading lower oceanic crust (Hess Deep, equatorial Pacific Ocean). *Earth and Planetary Science Letters, 361*, 436-447. doi:https://doi.org/10.1016/j.epsl.2012.11.012

Lissenberg, CJ, & Dick, H. J. (2008). Melt–rock reaction in the lower oceanic crust and its implications for the genesis of mid-ocean ridge basalt. *Earth and Planetary Science Letters, 271*(1-4), 311-325.

Marchildon, N., & Brown, M. (2002). Grain-scale melt distribution in two contact aureole rocks: Implications for controls on melt localization and deformation. *Journal of Metamorphic Geology, 20*(4), 381-396.

Milan, L., Daczko, N., & Clarke, G. (2017). Cordillera Zealandia: A Mesozoic arc flare-up on the palaeo-Pacific Gondwana Margin. *Scientific Reports, 7*(1), 261.

Milan, L., Daczko, N., Clarke, G., & Allibone, A. (2016). Complexity of in-situ zircon U–Pb–Hf isotope systematics during arc magma genesis at the roots of a Cretaceous arc, Fiordland, New Zealand. *Lithos, 264*, 296-314.

Morgan, Z., & Liang, Y. (2003). An experimental and numerical study of the kinetics of harzburgite reactive dissolution with applications to dunite dike formation. *Earth and Planetary Science Letters, 214*(1), 59-74. doi:https://doi.org/10.1016/S0012-821X(03)00375-3

Morgan, Z., & Liang, Y. (2005). An experimental study of the kinetics of lherzolite reactive dissolution with applications to melt channel formation. *Contributions to Mineralogy and Petrology, 150*(4), 369-385. doi:10.1007/s00410-005-0033-8

Mortimer, N., Tulloch, A., Spark, R., Walker, N., Ladley, E., Allibone, A., & Kimbrough, D. (1999). Overview of the Median Batholith, New Zealand: a new interpretation of the geology of the Median Tectonic Zone and adjacent rocks. *Journal of African earth sciences, 29*(1), 257-268.

Naney, M. (1983). Phase equilibria of rock-forming ferromagnesian silicates in granitic systems. *American Journal of Science, 283*(10), 993-1033.

Niida, K., & Green, D. H. (1999). Stability and chemical composition of pargasitic amphibole in MORB pyrolite under upper mantle conditions. *Contributions to Mineralogy and Petrology, 135*(1), 18-40. doi:10.1007/s004100050495

Pál-Molnár, E., Batki, A., Almási, E., Kiss, B., Upton, B. G., Markl, G., . . . Harangi, S. (2015). Origin of mafic and ultramafic cumulates from the Ditrău Alkaline Massif, Romania. *Lithos, 239*, 1-18.

Pandit, D., Panigrahi, M. K., & Moriyama, T. (2014). Constrains from magmatic and hydrothermal epidotes on crystallization of granitic magma and sulfide mineralization in Paleoproterozoic Malanjkhand Granitoid, Central India. *Chemie der Erde - Geochemistry, 74*(4), 715-733. doi:https://doi.org/10.1016/j.chemer.2014.04.008

Pec, M., Holtzman, B. K., Zimmerman, M. E., & Kohlstedt, D. L. (2017). Reaction Infiltration Instabilities in Mantle Rocks: an Experimental Investigation. *Journal of Petrology, 58*(5), 979-1003.

Piazolo, S., Bestmann, M., Prior, D., & Spiers, C. (2006). Temperature dependent grain boundary migration in deformed-then-annealed material: observations from experimentally deformed synthetic rocksalt. *Tectonophysics, 427*(1-4), 55-71.

Prakash, A., Piazolo, S., Saha, L., Bhattacharya, A., Pal, D. K., & Sarkar, S. (2018). Deformation behavior of migmatites: insights from microstructural analysis of a garnet–sillimanite–mullite–quartz–feldspar-bearing anatectic migmatite at Rampura–Agucha, Aravalli–Delhi Fold Belt, NW India. *International Journal of Earth Sciences*. doi:10.1007/s00531-018-1598-6

Prior, D. J., Wheeler, J., Peruzzo, L., Spiess, R., & Storey, C. (2002). Some garnet microstructures: an illustration of the potential of orientation maps and misorientation analysis in microstructural studies. *Journal of Structural Geology, 24*(6), 999-1011. doi:https://doi.org/10.1016/S0191-8141(01)00087-6

Putnis, A. (2009). Mineral replacement reactions. *Reviews in mineralogy and geochemistry, 70*(1), 87-124.

Rampone, Elisabetta, Borghini, G., Godard, M., Ildefonse, B., Crispini, L., & Fumagalli, P. (2016). Melt/rock reaction at oceanic peridotite/gabbro transition as revealed by trace element chemistry of olivine. *Geochimica et Cosmochimica Acta, 190*, 309-331. doi:https://doi.org/10.1016/j.gca.2016.06.029

Rampone, E., Piccardo, G., Vannucci, R., Bottazzi, P., & Zanetti, A. (1994). Melt impregnation in ophiolitic peridotite: an ion microprobe study of clinopyroxene and plagioclase. *Mineralogical Magazine A, 58*, 756-757.

Richet, P., Lejeune, A.-M., Holtz, F., & Roux, J. (1996). Water and the viscosity of andesite melts. *Chemical Geology, 128*(1-4), 185-197.

Roselle, G. T., Baumgartner, L. P., & Chapman, J. A. (1997). Nucleation-dominated crystallization of forsterite in the Ubehebe Peak contact aureole, California. *Geology, 25*(9), 823-826.

Rosenberg, C. L., & Riller, U. (2000). Partial-melt topology in statically and dynamically recrystallized granite. *Geology, 28*(1), 7-10. doi:10.1130/0091-7613(2000)28<7:ptisad>2.0.co;2

Rudnick, R. L. (1995). Making continental crust. *Nature, 378*, 571. doi:10.1038/378571a0

Sanfilippo, A., Morishita, T., Kumagai, H., Nakamura, K., Okino, K., Hara, K., . . . Arai, S. (2015). Hybrid troctolites from mid-ocean ridges: inherited mantle in the lower crust. *Lithos, 232*, 124-130. doi:https://doi.org/10.1016/j.lithos.2015.06.025

Sawyer, E. (1999). Criteria for the recognition of partial melting. *Physics and Chemistry of the Earth, Part A: Solid Earth and Geodesy, 24*(3), 269-279.

Sawyer, E. (2001). Melt segregation in the continental crust: distribution and movement of melt in anatectic rocks. *Journal of Metamorphic Geology, 19*(3), 291-309.

Schmidt, M. W., & Poli, S. (2004). Magmatic epidote. *Reviews in mineralogy and geochemistry, 56*(1), 399-430.

Schröter, F., Stevenson, J., Daczko, N., Clarke, G., Pearson, N., & Klepeis, K. (2004). Trace element partitioning during high-P partial melting and melt-rock interaction; an example from northern Fiordland, New Zealand. *Journal of Metamorphic Geology, 22*(5), 443-457.

Schubert, G., Turcotte, D. L., & Olson, P. (2001). *Mantle convection in the Earth and planets*: Cambridge University Press.

Schulmann, K., Martelat, J. E., Ulrich, S., Lexa, O., Štípská, P., & Becker, J. K. (2008). Evolution of microstructure and melt topology in partially molten granitic mylonite: Implications for rheology of felsic middle crust. *Journal of Geophysical Research: Solid Earth, 113*(B10).

Scott, D. R., & Stevenson, D. J. (1986). Magma ascent by porous flow. *Journal of Geophysical Research: Solid Earth, 91*(B9), 9283-9296.

Shaw, H. (1972). Viscosities of magmatic silicate liquids; an empirical method of prediction. *American Journal of Science, 272*(9), 870-893.

Sizova, E., Gerya, T., Stüwe, K., & Brown, M. (2015). Generation of felsic crust in the Archean: a geodynamic modeling perspective. *Precambrian Research, 271*, 198-224.

Sleep, N. H. (1988). Tapping of melt by veins and dikes. *Journal of Geophysical Research: Solid Earth, 93*(B9), 10255-10272. doi:10.1029/JB093iB09p10255

Smith, D. J. (2014). Clinopyroxene precursors to amphibole sponge in arc crust. *5*, 4329. doi:10.1038/ncomms5329

http://dharmasastra.live.cf.private.springer.com/articles/ncomms5329 - supplementary-information

Smith, J., Piazolo, S., Daczko, N., & Evans, L. (2015). The effect of pre-tectonic reaction and annealing extent on behaviour during subsequent deformation: insights from paired shear zones in the lower crust of Fiordland, New Zealand. *Journal of Metamorphic Geology, 33*(6), 557-577.

Solano, J. M. S., Jackson, M. D., Sparks, R. S. J., Blundy, J. D., & Annen, C. (2012). Melt Segregation in Deep Crustal Hot Zones: a Mechanism for Chemical Differentiation, Crustal Assimilation and the Formation of Evolved Magmas. *Journal of Petrology, 53*(10), 1999-2026. doi:10.1093/petrology/egs041

Spence, D. A., Sharp, P. W., & Turcotte, D. L. (1987). Buoyancy-driven crack propagation: a mechanism for magma migration. *Journal of Fluid Mechanics, 174*, 135-153. doi:10.1017/S0022112087000077

Spiegelman, M., Kelemen, P. B., & Aharonov, E. (2001). Causes and consequences of flow organization during melt transport: The reaction infiltration instability in compactible media. *Journal of Geophysical Research: Solid Earth, 106*(B2), 2061-2077.

Spruzeniece, L., Piazolo, S., Daczko, N., Kilburn, M., & Putnis, A. (2017). Symplectite formation in the presence of a reactive fluid: insights from hydrothermal experiments. *Journal of Metamorphic Geology, 35*(3), 281-299.

Spruzeniece, L., Piazolo, S., & Maynard-Casely, H. E. (2017). Deformation-resembling microstructure created by fluid-mediated dissolution–precipitation reactions. *Nature communications, 8*, 14032.

Stevenson, J. A., Daczko, N. R., Clarke, G. L., Pearson, N., & Klepeis, K. A. (2005). Direct observation of adakite melts generated in the lower continental crust, Fiordland, New Zealand. *Terra Nova, 17*(1), 73-79.

Štípská, P., Hasalová, P., Powell, R., Závada, P., Schulmann, K., Racek, M., . . . Chopin, F. (2019). The effect of melt infiltration on metagranitic rocks: The Snieznik dome, Bohemian Massif. *Journal of Petrology*.

Stowell, H., Tulloch, A., Zuluaga, C., & Koenig, A. (2010). Timing and duration of garnet granulite metamorphism in magmatic arc crust, Fiordland, New Zealand. *Chemical Geology, 273*(1), 91-110.

Streit, J. E., & Cox, S. F. (1998). Fluid infiltration and volume change during mid-crustal mylonitization of Proterozoic granite, King Island, Tasmania. *Journal of Metamorphic Geology, 16*(2), 197-212. doi:10.1111/j.1525-1314.1998.00129.x

Stuart, C. A., Daczko, N. R., & Piazolo, S. (2017). Local partial melting of the lower crust triggered by hydration through melt–rock interaction: an example from Fiordland, New Zealand. *Journal of Metamorphic Geology, 35*(2), 213-230.

Stuart, C. A., Meek, U., Daczko, N. R., Piazolo, S., & Huang, J. X. (2018). Chemical Signatures of Melt–Rock Interaction in the Root of a Magmatic Arc. *Journal of Petrology, 59*(2), 321-340. doi:10.1093/petrology/egy029

Stuart, C. A., Piazolo, S., & Daczko, N. R. (2016). Mass transfer in the lower crust: Evidence for incipient melt assisted flow along grain boundaries in the deep arc granulites of Fiordland, New Zealand. *Geochemistry, Geophysics, Geosystems, 17*(9), 3733-3753. doi:10.1002/2015GC006236

Stuart, C. A., Piazolo, S., & Daczko, N. R. (2018). The recognition of former melt flux through high-strain zones. *Journal of Metamorphic Geology, 36*(8), 1049-1069. doi:doi:10.1111/jmg.12427

Tetley, M., & Daczko, N. (2014). Virtual Petrographic Microscope: a multi-platform education and research software tool to analyse rock thin-sections. *Australian Journal of Earth Sciences, 61*(4), 631-637.

Turcotte, D., & Ahern, J. (1978). A porous flow model for magma migration in the asthenosphere. *Journal of Geophysical Research: Solid Earth, 83*(B2), 767-772.

Vanderhaeghe, O. (1999). Pervasive melt migration from migmatites to leucogranite in the Shuswap metamorphic core complex, Canada: control of regional deformation. *Tectonophysics, 312*(1), 35-55.

Vernon, R. (2011). Microstructures of melt-bearing regional metamorphic rocks. *Geological Society of America Memoirs, 207*, 1-11.

Wade, J., Dyck, B., Palin, R. M., Moore, J. D. P., & Smye, A. J. (2017). The divergent fates of primitive hydrospheric water on Earth and Mars. *Nature, 552*, 391. doi:10.1038/nature25031

Weinberg, R.F. (1996). Ascent mechanism of felsic magmas: news and views. *Geological Society of America Special Papers, 315*, 95-103.

Weinberg, R.F. (1999). Mesoscale pervasive felsic magma migration: alternatives to dyking. *Lithos, 46*(3), 393-410.

Weinberg, RF, & Searle, M. (1998). The Pangong Injection Complex, Indian Karakoram: a case of pervasive granite flowthrough hot viscous crust. *Journal of the Geological Society, 155*(5), 883-891.

Wu, K., Ling, M. X., Hu, Y. B., Guo, J., Jiang, X. Y., Sun, S. J., . . . Sun, W. (2018). Melt-Fluxed Melting of the Heterogeneously Mixed Lower Arc Crust: A Case Study from the Qinling Orogenic Belt, Central China. *Geochemistry, Geophysics, Geosystems, 19*(6), 1767-1788.

Závada, P., Schulmann, K., Konopásek, J., Ulrich, S., & Lexa, O. (2007). Extreme ductility of feldspar aggregates—Melt-enhanced grain boundary sliding and creep failure: Rheological implications for felsic lower crust. *Journal of Geophysical Research: Solid Earth, 112*(B10).

Závada, P., Schulmann, K., Racek, M., Hasalová, P., Jeřábek, P., Weinberg, R. F., . . . Roberts, A. (2018). Role of strain localization and melt flow on exhumation of deeply subducted continental crust. *Lithosphere, 10*(2), 217-238.

Zen, E.-A., & Hammarstrom, J. M. (1984). Magmatic epidote and its petrologic significance. *Geology, 12*(9), 515-518.

FIGURE CAPTIONS

Figure 1. Field relationships of the hornblende-rich bodies studied, Pembroke Valley, Fiordland, New Zealand. a) Aerial view of the site 1 hornblende-rich body (H, white dashed lines) hosted within two-pyroxene-pargasite gneiss. Structural map 1b marked by white rectangle. Inset: locality of field area (red star) within northern part of the Fiordland Magmatic Provenance (black). b) Structural field map of the site 1 hornblende-rich body, showing hornblende-rich body (H), surrounded by a hydration halo termed Transition Zone (TZ) within two-pyroxene-pargasite, gabbroic gneiss (GG) c),d), Field photographs of site 2 hornblende-rich body, surrounded by TZ, located a few hundred metres lower in the valley. This body is much thinner than the site 1 hornblende-rich body; note camera cap (diameter 5 cm) for scale.

Figure 2: Field relationships and microstructures of the two pyroxene-pargasite-gneiss, gabbroic gneiss (GG) which forms the host and precursor rock. a) Outcrop photograph of the host with S_1 gneissosity, featuring rectilinear garnet reaction zones (GRZ). Inset shows gneissosity is unaffected by GRZ i.e. it is continuous from host into GRZ. b) Photomicrograph showing mafic clusters of enstatite, diopside and pargasite defining the S_1 gneissosity, hosted within a predominantly plagioclase-rich matrix, plane polarised light, c) Photomicrograph of a garnet reaction zone (GRZ), showing partial replacement of diopside and enstatite by garnet, plane polarised light.

Figure 3: Field characteristics of the hornblende-rich body. a) Clinozoisite-hornblendite (>10% cz, H(Cz-Hbl)) and hornblendite (H(Hbl)) (<10% cz)), contact highlighted by dashed

white line. Garnetite stringers are present in both rock units (double white arrows). b) Pegmatite bodies within, and enclosing, both H(Hbl) and H(Cz-Hbl) (inset). Pegmatite consists of coarse-grained hornblende (yellow arrows), garnet (white arrows) and plagioclase (red arrows). Garnetite stringers found throughout. The boundaries of the pegmatite are diffuse. c) Close-up of garnetite stringer predominantly consisting of garnet (H(Grt)) within hornblende-rich body, large 1 cm wide garnet porphryoblasts (white arrow) are present. d) Garnet porphryoblasts within the transition zone (white arrows), close to the boundary of the two units (separated by white dashed lines). Inset shows several garnet euhedral porphryoblasts which are surrounded by thin felsic rims; a common feature within the TZ; garnet is up to 10 cm wide.

Figure 4: Field characteristics of the transition zone and hornblende-rich body relationship. a) Modified garnet reaction zones (GRZ) in transition zone. Garnet surrounded by either plagioclase or hornblende (white arrows) or both (red arrows). Contact boundary highlighted by white dashed line. b) Highly irregular contact boundary between hornblende-rich body (H) and TZ. In this area, H protrudes out in a finger-like pattern, often linked to modified GRZ in the TZ. c) Another hornblende-rich body in the valley with protrusions at the TZ-H boundary. d) Regular contact boundary between H and TZ (white line) as is the contact between TZ and GG (black line). e) Large lozenge-shaped TZ “remnants” within the H body (also refer to Fig. 1b). f) Small rounded TZ “remnant” within H (near H-TZ boundary) where garnetite stringers appear to deflect around (double white arrows). Porphyroblastic garnet abundant here (white arrows).

Figure 5: Field characteristics of the GRZ and their relationship to different main lithologies. a) Field map of close-up relationships of the northern side of the hornblende-rich body (area marked in Fig. 1b). Modified GRZ (grey) within the transition zone swing in and become sub-parallel to the hornblende-rich body, as a result of sinistral shearing. Several of these

modified GRZ can be traced directly into the hornblende-rich body where they are transformed to garnetite stringers (white), and are intensely deformed, dismembered and folded. Porphyroblastic garnets found throughout the TZ. b) Field map of the southern side of the hornblende-rich body (area marked in Fig. 1b; note: GRZ within the two-pyroxene-pargasite gneiss in three orientations (light grey). GRZ perpendicular to the hornblende-rich body are bent due to strain from sinistral shearing. They are complexly deformed within the TZ (grey) and some lead directly into the hornblende-rich body (white). Porphyroblastic garnets found throughout the TZ. c) Close-up of modified GRZ within the TZ; these are typically surrounded by either hornblende (upper) or plagioclase (lower). d) Modified GRZ; note that a single GRZ may be surrounded by hornblende (hbl) and then plagioclase (pl) along strike. e) Modified GRZ seen within the hornblende-rich body where they are now garnetite stringers. In this image, garnetite stringers preserve orientation relationships closely resembling those seen in the host rock; i.e. they are rectilinear. f), g), h) Garnetite stringers are variably deformed, where they show apparent “M” folds (f), “S” and “Z” open to tight folds (g), to sheath folds (h).

Figure 6: Whole rock geochemistry of gabbroic gneiss (1 sample) transition zone (1 sample), clinozoisite-hornblendite (3 samples) and hornblendite (3 samples). Harker style diagram with SiO_2 content on the x-axis and weight percent oxide (wt. %) for Fe_2O_3, Na_2O and MgO on the y-axis. LOI values presented by white box per sample with values corresponding to right-hand side.

Figure 7: Microstructural characteristics of clinozoisite-hornblendite rock and garnetite stringer a) Photomicrograph in plane polarised light of clinozoisite-hornblendite H(Cz-Hbl) and a garnetite stringer H(Grt). Scale bar is 1mm. BSE and EBSD areas are marked and boundary between the two is outlined by a dashed line. b) BSE of H(Cz-Hbl) area showing interstitial plagioclase (pl) films along grain boundaries of both clinozoisite (cz) and

hornblende (hbl). White arrows indicate dihedral angles as low as <10°. Inset shows crystallographic orientation map for pl, (cz and hbl phase colours), note plagioclase is not connected in 2D but has the same crystallographic orientation, hence must be connected in 3D. Area for c) marked. c) Inclusions within cz grain are often hbl (see a)). However, in this area they are multiphase crystallisations. d) EBSD based phase map of clinozoisite-hosted multiphase inclusion mineral phases (cz, pl, hbl, clinochlore, K-feldspar), scale bar 50 μm. e) crystallographic orientation map of clinozoisite-hosted multiphase inclusions. Cz host and cz within inclusions have same orientation. Pl twin set (noted) and hbl each have their own orientation that is the same (i.e. there is one main pl twin set, hbl has the same orientation throughout). Clinochlore exhibits the same orientation where found. Sale bar 50 μm. f) & g) Example BSE images of low dihedral angles of pl, where white arrows indicate angles as low as 10°. Scale bars 100 μm. h) BSE image of contact with garnetite stringer. Note irregularly shaped plagioclase grain with some very low dihedral angles of plagioclase and hornblende (white arrows). Hosted within the plagioclase is rutile (rt) and apatite (ap). i) Crystallographic orientation map for plagioclase, note plagioclase is a single grain with a consistent twin set orientation (see pole figure, twin shown by colours).

Figure 8: Microstructural characteristics of hornblendite and garnetite stringer. a) Photomicrograph plane polarised light of hornblendite H(Hbl) and a garnetite stringer H(Grt). Scale bar is 1mm. BSE and EBSD areas are marked. b) BSE of multiphase crystallisations found within hornblendite. Note very low dihedral angles at several ends, <10° (white arrows). Phases found are plagioclase (pl), biotite (bt), garnet (grt) and rutile (rt). Note that plagioclase is irregularly shaped. Bt have nice crystal faceting and garnet has corroded crystal shapes. c) EBSD-based phase map. d) Same area as shown in (c), crystallographic orientations for plagioclase and garnet shown as varying colours; hornblende is shown as a

phase in green. Note there are two main plagioclase twin sets that are found (marked). Garnet orientation colouring and pole figure shows garnet grains have the same orientation.

Figure 9: Microstructural characteristics of garnetite stringers within hornblende-rich body. a) BSE image of garnetite stringer showing garnet (grt), hornblende (hbl) grains and interstitial plagioclase (pl), and minor ilmenite (ilm). White arrows point to very low dihedral angles of plagioclase and hornblende (<10°). Box outlines area of b-d. b) Garnet (red) and hornblende (green) with interstitial plagioclase. Plagioclase crystallographic orientation colouring shows two interconnected grain networks (black arrows, 1 & 2) where plagioclase grains not connected in 2D show the same orientation, hence must be connected in 3D. c) Garnet (red) and plagioclase (blue) as phase colours. Crystallographic orientations of hornblende show three separate grains which each exhibit anhedral hornblende crystal shapes. d) Hornblende and plagioclase, from above, in white. Garnet crystallographic orientation colouring shows a mix of rounded garnets, to amoeboidal grain shapes and sub-grains. Severe lattice distortion showing no systematic preference of orientation are highlighted with low degree boundaries. A <111> pole figure of blue strongly distorted grain shows an irregular orientation spread, within slightly distorted intracrystal misorientations. Comparatively, crystallographic orientations of all garnet grains (as one point per grain) showing there is a lack of preferred orientation across garnetite stringers; note that the same colour scheme is used in the pole figures and (d). e) Hornblende and plagioclase (from 7h) in phase colours. Crystallographic orientation colouring shown for garnet only. Note lattice distortions within individual grains.

Figure 10: Microstructural characteristics of hornblendite (Hbl) – transition zone (TZ) boundary. a) Photomicrograph showing boundary, plane polarised light; note S_1 gneissosity; scale bar is 1 cm and SEM and EBSD areas are marked as black boxes. b) Plagioclase orientation map shows two main plagioclase grains within the transition zone. Two main twin sets reveal deformation twinning with tapered twins. Small plagioclase grains show no

deformation twinning or other deformation features (inset). Remnant islands of plagioclase grains found enclosed within hornblende are shown with black arrows; c) Hornblende orientation colour map (inset, BSE image of EBSD area with shape marked). Note various crystallographic orientations of hornblende grains, independent of the plagioclase grain it surrounds. Hornblende is found surrounding plagioclase and at triple junctions (top, smaller grains) and at a plagioclase twin boundary. Similar to b) small grains showing random orientations occur at pl-hbl boundaries. d) BSE image near contact boundary, marked in a) showing enclosure of plagioclase grain in hornblende grain. e) Hornblende in white and plagioclase crystallographic orientations shown. Note a remnant sub-grain of plagioclase, surrounded by hornblende (black arrow). Hornblende has irregular cuspate-lobate boundaries, atypical of hornblende crystal shapes.

Figure 11: Evolution of the microstructure with increasing melt flux leading to the identified microstructural characteristics. Stage 1: Externally-derived melt infiltrates the pre-existing gabbroic gneiss via porous melt flow (likely deformation-assisted), where melt moves along grain boundaries; Stage 2: at the immediate contact boundary between the transition zone and hornblende-rich body; (i) remnant islands of old plagioclase sub-grains, (ii) local precipitation of new, fine-grained plagioclase of evolving composition, (iii) some equilibrated hornblende-plagioclase boundaries, (iv) pointed melt films at melt front, and (v) highly irregular hornblende-plagioclase grain boundaries along reaction front. Stage 3: During increased melt flux and melt-rock reactions, microstructures evolve from µm-mm scale instabilities to subhedral to anhedral, igneous-like crystal faces of hornblende and clinozoisite. Clinozoisite with hornblende inclusions, due to coeval crystallisation, and garnetite. Microstructures indicative of the former presence of melt include (vi) plagioclase melt films along grain boundaries, some with low dihedral angles as low as $<10^{\circ}$ (where growth twin crystallographic orientations indicate interconnected 3D melt networks), (vii) plagioclase and hornblende films

within garnetite, with some low dihedral angles, (viii) melt pocket crystallisations and (ix) severe crystallographic lattice distortions.

TABLE CAPTIONS

Table 1. Characteristics of the main rock types of this study.

SUPPORTING INFORMATION

Additional Supporting Information may be found in the online version of this article at the publisher's web site:

Figure S1. Histogram of measured apparent low dihedral angles (200 measurements). Note that some apparent low dihedral angles are as low as <10° and that there is a relatively even spread of apparent low dihedral angles between those <10° and those <60°. BSE images from which the apparent low dihedral angles were measured are shown as examples. White arrows point to the examples of measured angles.

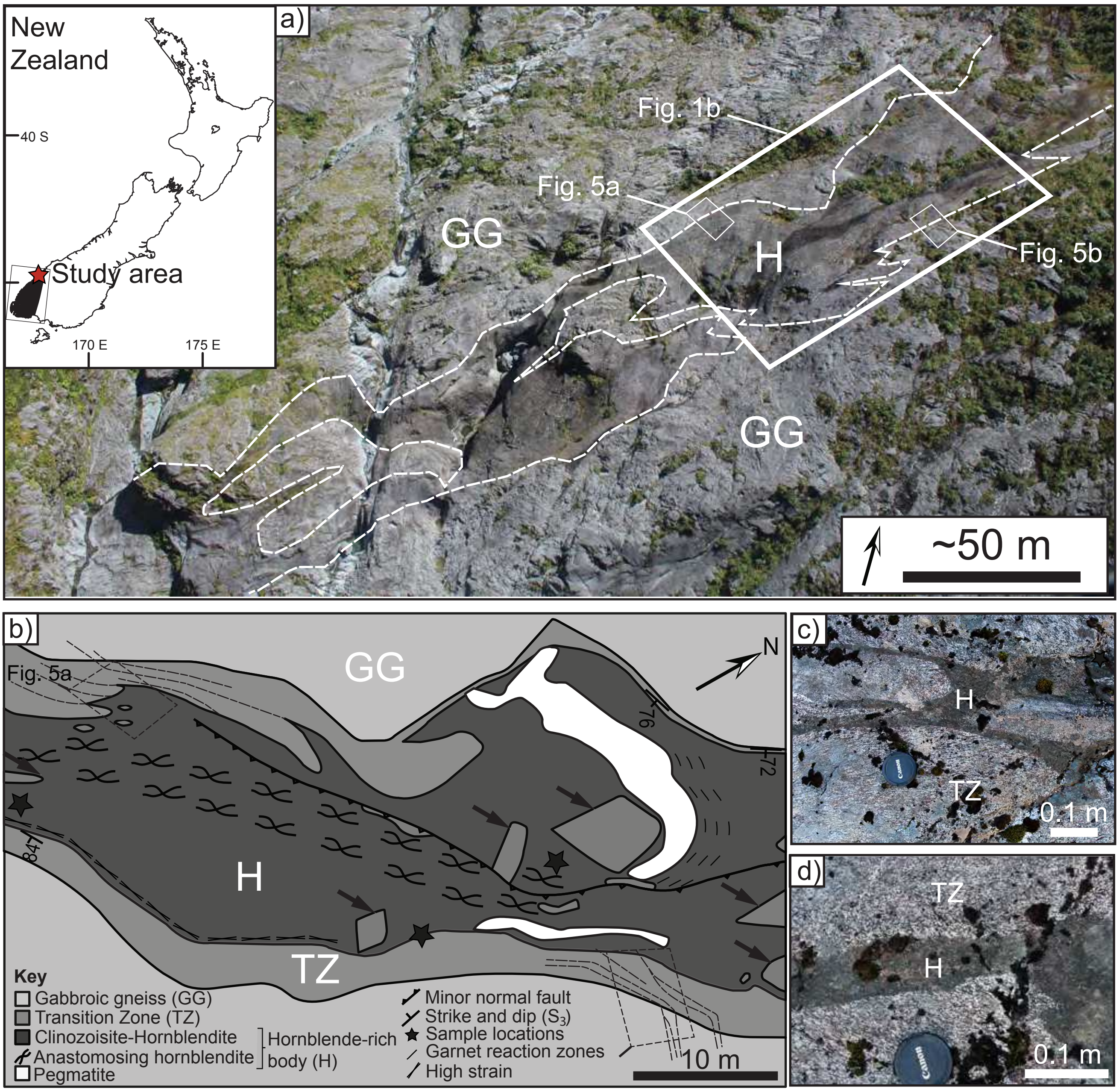
a)
New Zealand
40 S
Study area
170 E
175 E
Fig. 1b
Fig. 5a
Fig. 5b
GG
H
GG
~50 m
b)
Fig. 5a
GG
N
H
TZ
76
72
84
Key
Gabbroic gneiss (GG)
Transition Zone (TZ)
Clinozoisite-Hornblendite
Anastomosing hornblendite
Pegmatite
Hornblende-rich body (H)
Minor normal fault
Strike and dip (S_3)
Sample locations
Garnet reaction zones
High strain
10 m
c)
H
TZ
0.1 m
d)
TZ
H
0.1 m

Figure 1

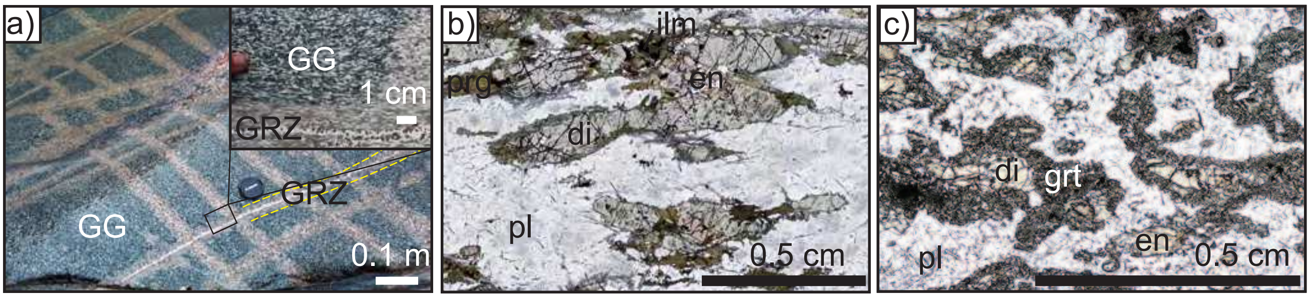

Figure 2

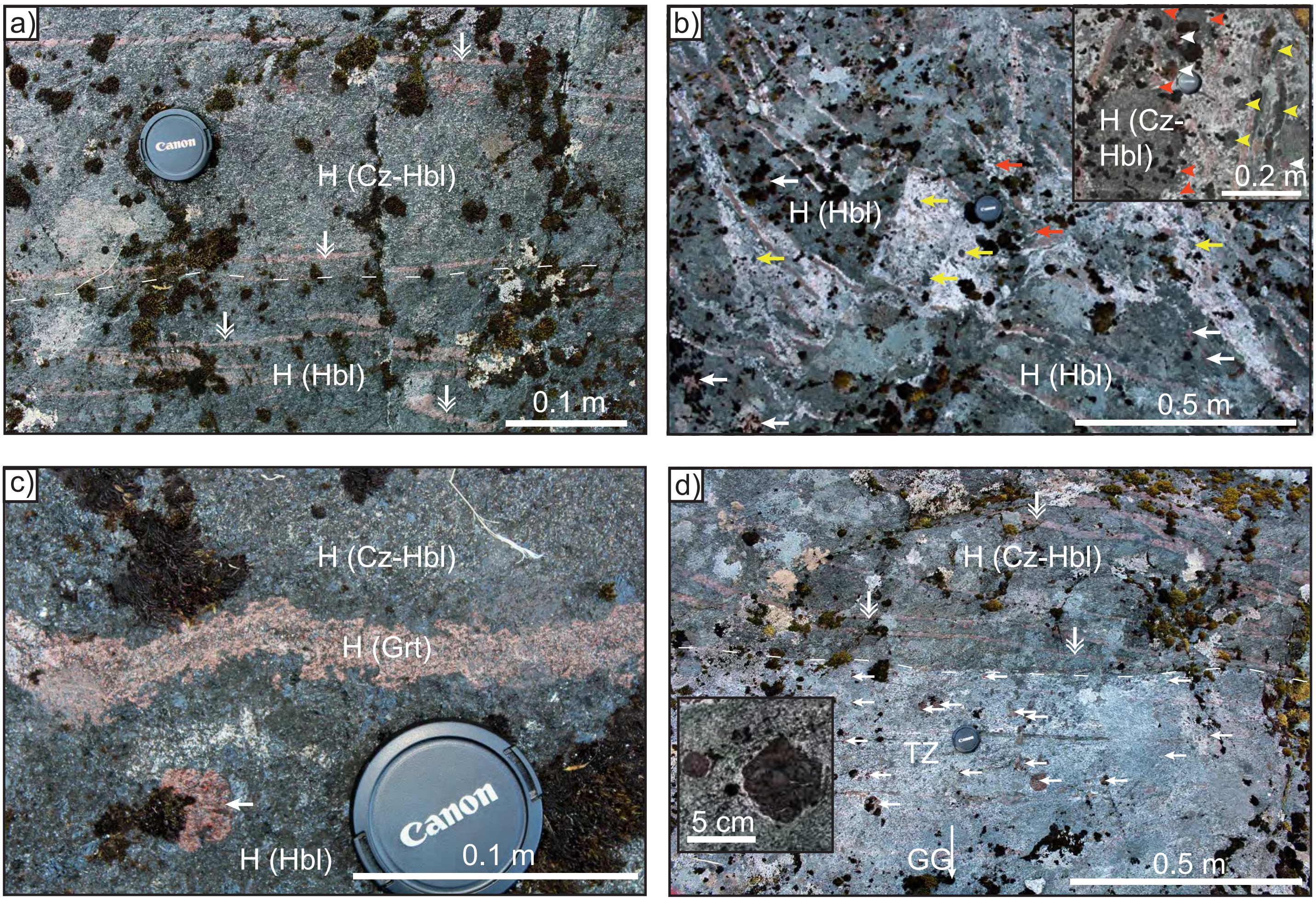

a)
H (Cz-Hbl)
H (Hbl)
0.1 m
b)
H (Hbl)
H (Hbl)
0.5 m
H (Cz-Hbl)
0.2 m
c)
H (Cz-Hbl)
H (Grt)
H (Hbl)
0.1 m
d)
H (Cz-Hbl)
TZ
GG
5 cm
0.5 m

Figure 3

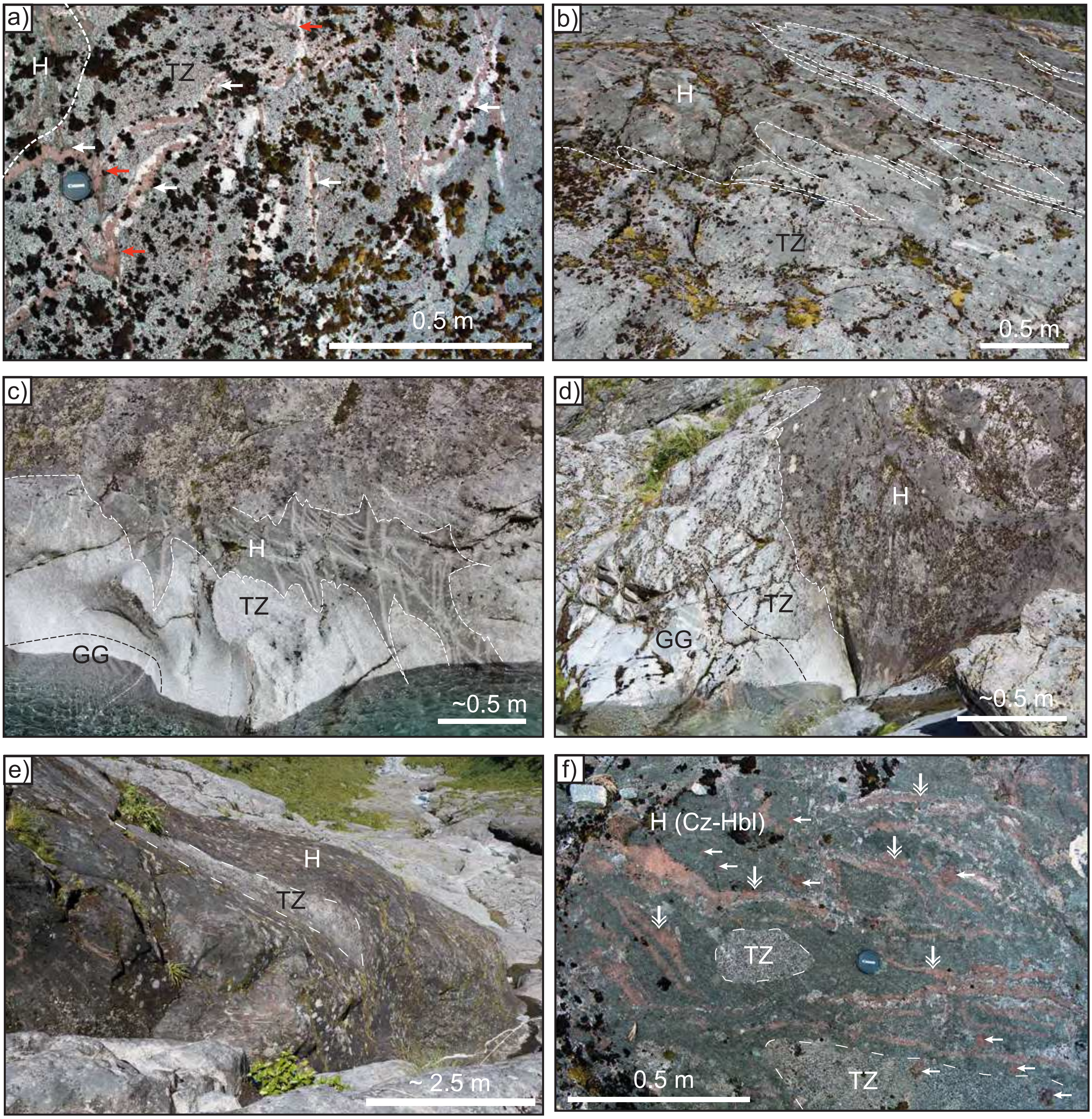
a)
H
TZ
0.5 m
b)
H
TZ
0.5 m
c)
H
TZ
GG
~0.5 m
d)
H
TZ
GG
~0.5 m
e)
H
TZ
~ 2.5 m
f)
H (Cz-Hbl)
TZ
TZ
0.5 m

Figure 4

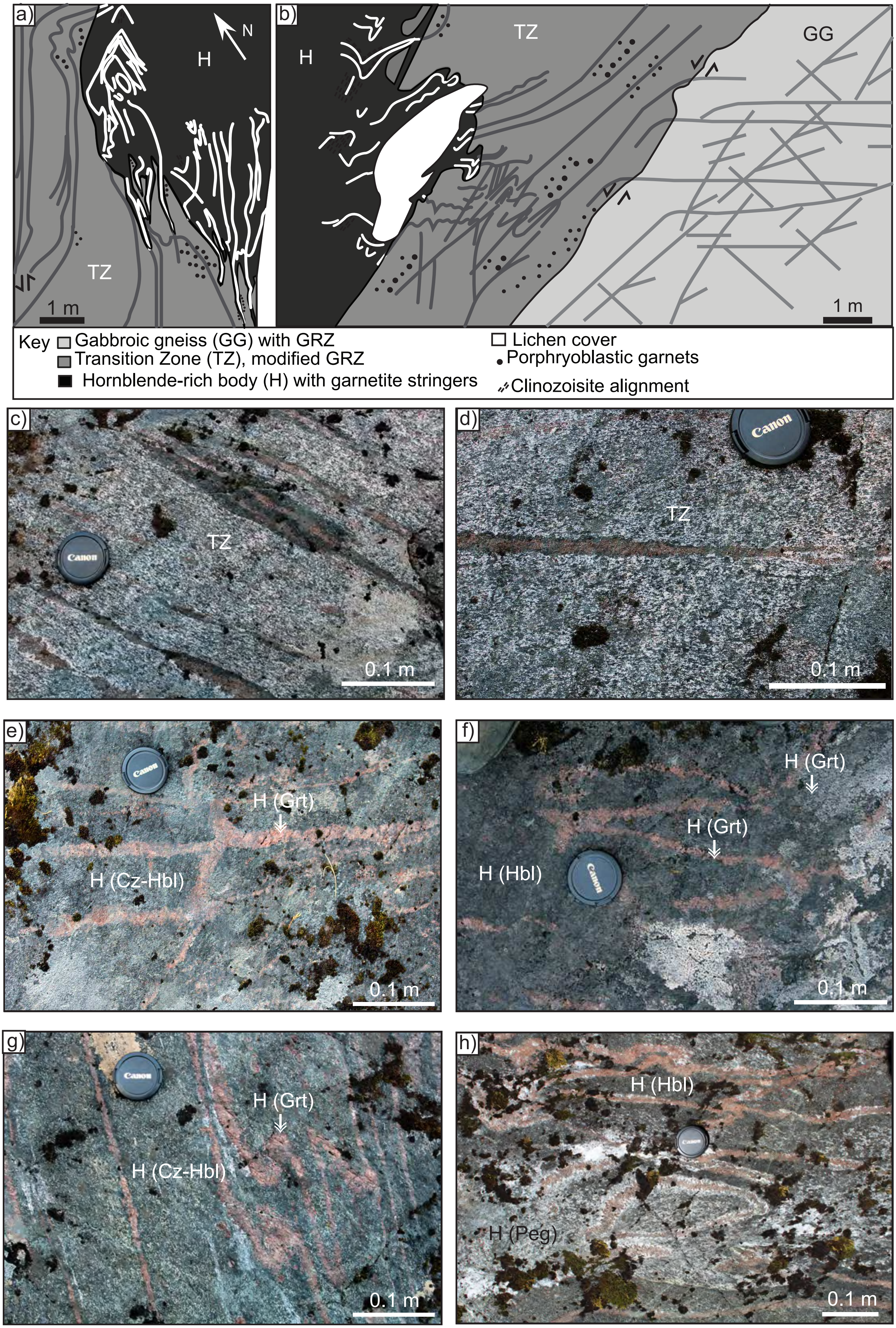
a)
H
N
TZ
1 m
b)
H
TZ
GG
1 m
Key
Gabbroic gneiss (GG) with GRZ
Transition Zone (TZ), modified GRZ
Hornblende-rich body (H) with garnetite stringers
Lichen cover
Porphryoblastic garnets
Clinozoisite alignment
c)
TZ
0.1 m
d)
TZ
0.1 m
e)
H (Grt)
H (Cz-Hbl)
0.1 m
f)
H (Grt)
H (Grt)
H (Hbl)
0.1 m
g)
H (Grt)
H (Cz-Hbl)
0.1 m
h)
H (Hbl)
H (Peg)
0.1 m

Figure 5

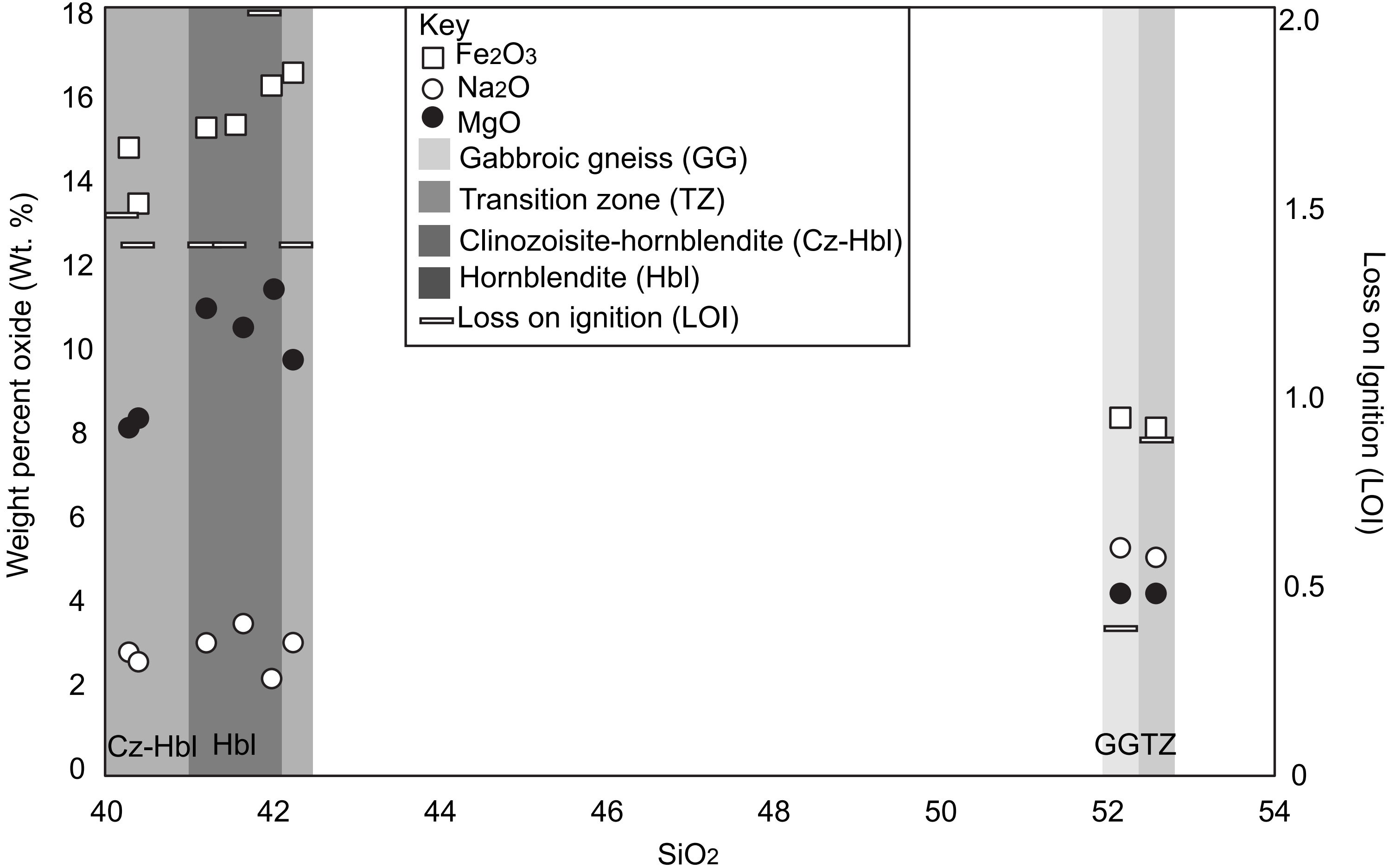
Key
Fe2O3
Na2O
MgO
Gabbroic gneiss (GG)
Transition zone (TZ)
Clinozoisite-hornblendite (Cz-Hbl)
Hornblendite (Hbl)
Loss on ignition (LOI)
Weight percent oxide (Wt. %)
Loss on Ignition (LOI)
SiO2
Cz-Hbl
Hbl
GG
TZ
0
2
4
6
8
10
12
14
16
18
0.5
1.0
1.5
2.0
40
42
44
46
48
50
52
54

Figure 6

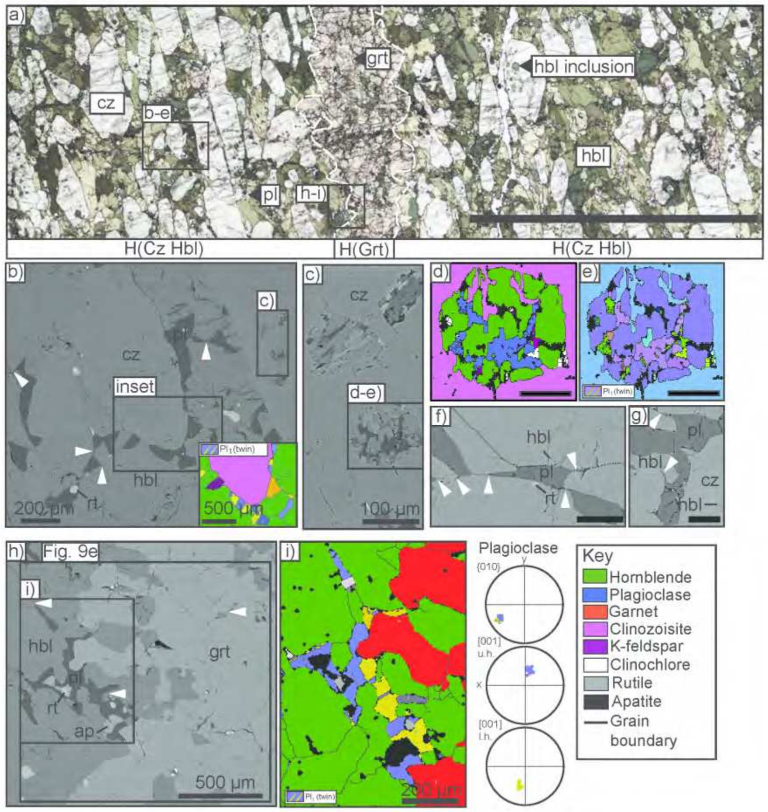

Figure 7

215x279mm (300 x 300 DPI)

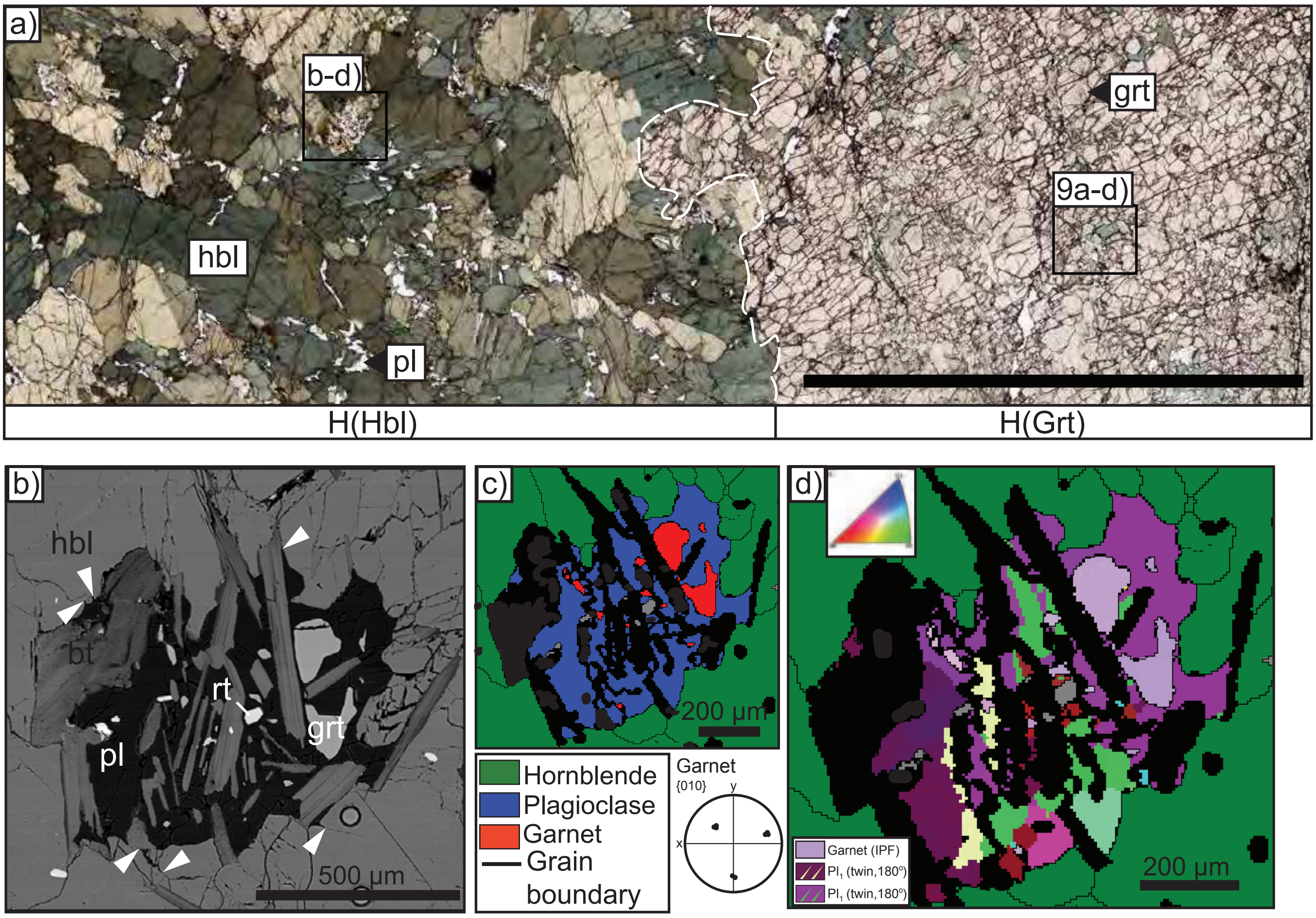
a)
b-d)
grt
9a-d)
hbl
pl
H(Hbl)
H(Grt)
b)
hbl
bt
rt
pl
grt
500 µm
c)
200 µm
Hornblende
Plagioclase
Garnet
Grain boundary
Garnet
{010}
y
x
d)
Garnet (IPF)
Pl1 (twin,180°)
Pl1 (twin,180°)
200 µm

Figure 8

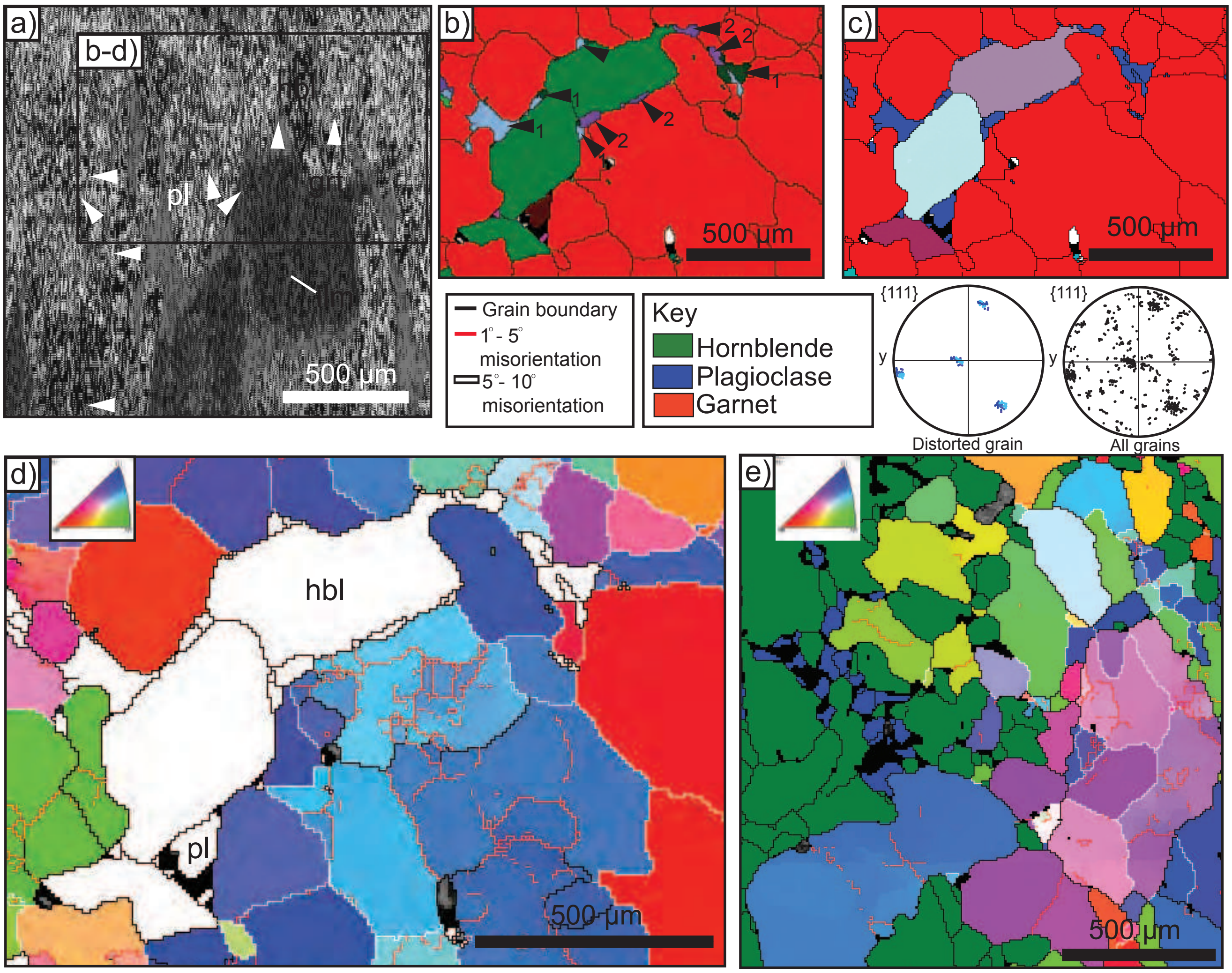
a)
b-d)
pl
500 µm
b)
1
2
500 µm
c)
500 µm
Grain boundary
1° - 5° misorientation
5° - 10° misorientation
Key
Hornblende
Plagioclase
Garnet
{111}
y
Distorted grain
All grains
d)
hbl
pl
500 µm
e)
500 µm

Figure 9

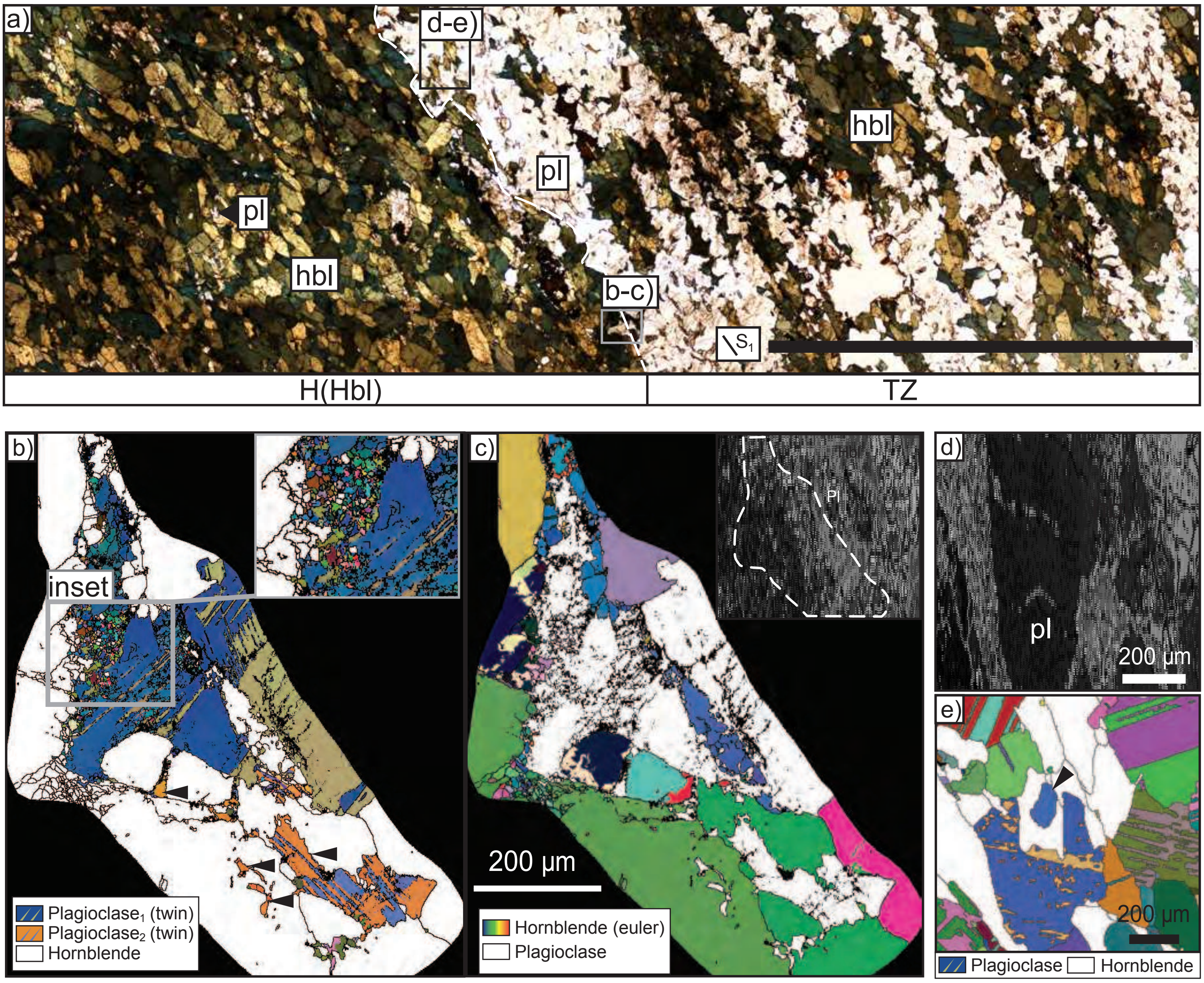
a)
d-e)
hbl
pl
pl
hbl
b-c)
S1
H(Hbl)
TZ
b)
inset
Plagioclase1 (twin)
Plagioclase2 (twin)
Hornblende
c)
Pl
200 µm
Hornblende (euler)
Plagioclase
d)
pl
200 µm
e)
200 µm
Plagioclase
Hornblende

Figure 10

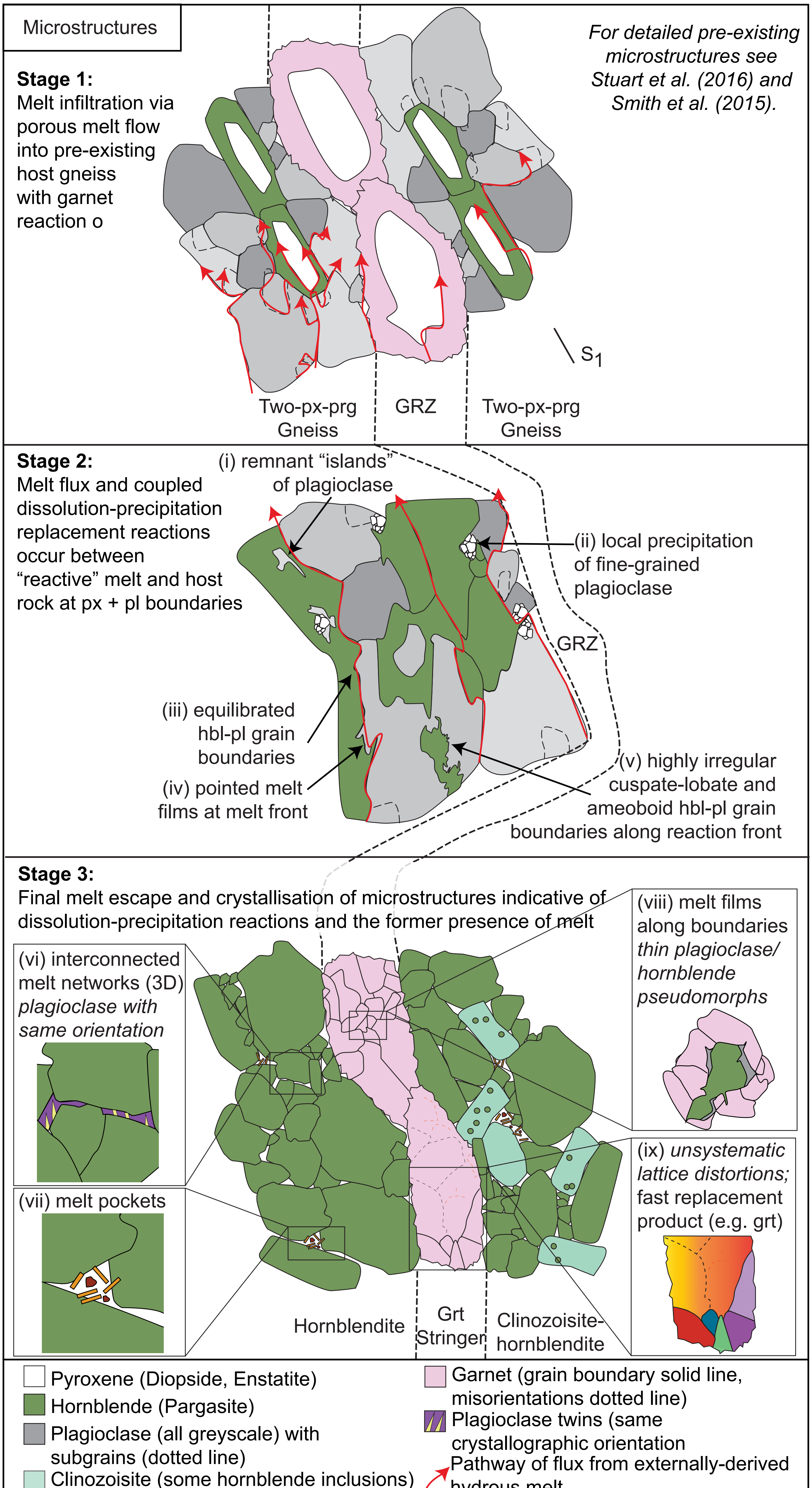
Microstructures
Stage 1:
Melt infiltration via porous melt flow into pre-existing host gneiss with garnet reaction o
For detailed pre-existing microstructures see Stuart et al. (2016) and Smith et al. (2015).
S1
Two-px-prg Gneiss
GRZ
Two-px-prg Gneiss
Stage 2:
Melt flux and coupled dissolution-precipitation replacement reactions occur between “reactive” melt and host rock at px + pl boundaries
(i) remnant “islands” of plagioclase
(ii) local precipitation of fine-grained plagioclase
GRZ
(iii) equilibrated hbl-pl grain boundaries
(iv) pointed melt films at melt front
(v) highly irregular cuspate-lobate and ameoboid hbl-pl grain boundaries along reaction front
Stage 3:
Final melt escape and crystallisation of microstructures indicative of dissolution-precipitation reactions and the former presence of melt
(vi) interconnected melt networks (3D) plagioclase with same orientation
(vii) melt pockets
(viii) melt films along boundaries thin plagioclase/ hornblende pseudomorphs
(ix) unsystematic lattice distortions; fast replacement product (e.g. grt)
Hornblendite
Grt Stringer
Clinozoisite-hornblendite
Pyroxene (Diopside, Enstatite)
Hornblende (Pargasite)
Plagioclase (all greyscale) with subgrains (dotted line)
Clinozoisite (some hornblende inclusions)
Garnet (grain boundary solid line, misorientations dotted line)
Plagioclase twins (same crystallographic orientation
Pathway of flux from externally-derived hydrous melt

Figure 11

Table 1. Characteristics of the main rock types of this study.

Rock unit	**Rock type**	**Mineralogy (area %)**	**Ductile features**	**Presence of GRZ (original bold, modified italic)**	**Microstructures indicative of the former presence of melt**
Gabbroic Gneiss (GG)	*Two pyroxene-pargasite gneiss*	~45 pl 20 hbl (± minor qtz sym) ~15 cpx ~10 opx Minor cz, ky, ap, ru, ilm	Yes - S_1 magmatic foliation	**GRZ**	No
Hornblende-rich body (H)	*Clinozoisite-hornblendite (H(Cz-Hbl)*	10–50 cz 50–95 hbl Minor pl, grt	No	*GRZ*	Yes - pl films - 3D networks - melt pocket
	Hornblendite (H(Hbl))	95 hbl Minor pl, grt	No	*GRZ*	Yes - pl films - 3D networks - melt pocket
	Garnetite	90–95 grt Minor hbl, pl	No	*GRZ*	Yes - pl/hbl films - 3D networks - grt lattice distortion
Transition Zone (TZ)	*Hornblende-feldspar gneiss*	~45 pl 45 hbl (± minor qtz sym) Minor cz, ky, ap, ru, ilm	Yes - S_1 magmatic foliation - S_3 shear zone foliation	*GRZ*	Yes - large grt with surrounding leucosome -unreacted remnant bodies

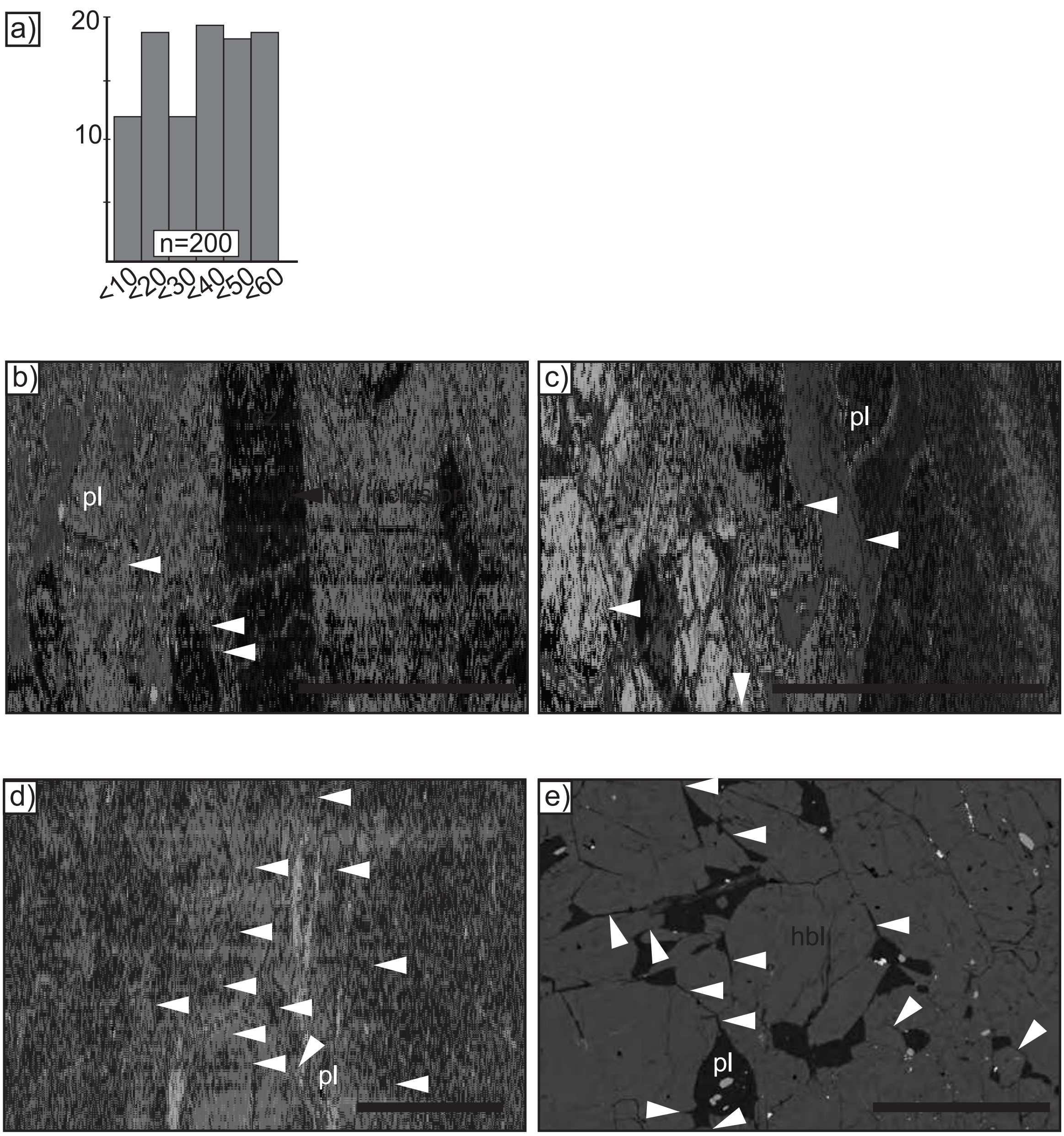
a)
20
10
n=200
<10
<20
<30
<40
<50
<60
b)
pl
c)
pl
d)
pl
e)
hbl
pl